Espoo, Finland 2006

SELF-ASSEMBLED NANORINGS AND STRESSOR QUANTUM DOTS

Doctoral Dissertation

Juha Riikonen

Dissertation for the degree of Doctor of Science in Technology to be presented with due permission of the Department of Electrical and Communications Engineering for public examination and debate in Auditorium AS1 at Helsinki University of Technology (Espoo, Finland) on the 2nd of June, 2006, at 12 noon.

Helsinki University of Technology
Department of Electrical and Communications Engineering
Optoelectronics Laboratory

Teknillinen korkeakoulu
Sähkö- ja tietoliikennetekniikan osasto
Optoelektroniikan laboratorio

Distribution:
Helsinki University of Technology
Department of Electrical and Communications Engineering
Optoelectronics Laboratory
P.O. Box 3500
FIN-02015 TKK
FINLAND
Tel: +358 9 4511
Fax: +358 9 451 3128
E-mail: juha.riikonen@tkk.fi
© 2006 Juha Riikonen

ISBN 951-22-8181-3 (printed version)
ISBN 951-22-8182-1 (electronic version)
URL: http://lib.tkk.fi/Diss/2006/isbn9512281821/

Otamedia Oy
Espoo 2006

ABSTRACT OF DOCTORAL DISSERTATION

HELSINKI UNIVERSITY OF TECHNOLOGY
P. O. BOX 1000, FI-02015 TKK
http://www.tkk.fi

Author Juha Riikonen

Name of the dissertation
Self-assembled nanorings and stressor quantum dots

Date of manuscript 23rd January 2006	Date of the dissertation 2nd June 2006
Article dissertation (overview + original articles)	Number of pages 56+62

Department	Department of Electrical and Communications Engineering
Laboratory	Optoelectronics laboratory
Field of research	Nanotechnology
Opponent	Prof. Srinivasan Anand
Supervisor	Prof. Harri Lipsanen

Abstract

In this thesis, the main focus is in the fabrication and characterization of self-assembled III-V compound semiconductor nanostructures. The samples were fabricated by metalorganic vapor phase epitaxy (MOVPE). Atomic force microscopy (AFM) and photoluminescence (PL) measurements were used to examine surface morphology and optical characteristics of the samples, respectively.

Quantum dot (QD) heterostructures are typically realized by embedding self-assembled islands in a matrix of another semiconductor material with a higher band gap. In this work, however, islands were used as stressors on top of a near-surface quantum well (QW) to induce three-dimensional potential enclosures into the QW. These QD structures are known as strain-induced QDs (SIQDs) or stressor QDs. Firstly, a new material system utilizing InAs stressor islands to create strain-induced InGaAs(P)/InP QDs was demonstrated. Up to four PL peaks from the QD ground and excited states were clearly resolved in the spectra. The island ensemble was optimized using a growth temperature ramp-down during the InAs island deposition. The luminescence wavelength was tuned by varying the QW composition. On the other hand, the QD confinement was modified by altering the height of the stressor islands or by varying the distance of the QW from the surface.

Secondly, transformation of self-assembled InAs islands into volcano-like nanorings was investigated. In the method introduced in this thesis, contrary to previous techniques utilizing partial capping of islands, only phosphorus annealing was applied. It is assumed that the material redistribution, i.e., the island-to-ring transformation, is caused by the exchange of As atoms to P atoms along with the strain-driven migration of In atoms outwards from the island.

Thirdly, surface passivation of GaAs by an *in situ* grown epitaxial ultrathin GaN layer was studied. Near-surface InGaAs/GaAs QWs were used as low-dimensional test structures, on which the passivation was applied. PL measurements were used to assess the effect of the passivation. Significant enhancement of the PL intensity shows that the growth of an ultrathin GaN layers is an efficient method in the passivation of GaAs surfaces.

Keywords MOVPE, epitaxy, nanotechnology, self-assembled, compound semiconductor, quantum dot, nanoring, quantum ring, passivation

ISBN (printed) 951-22-8181-3	ISBN (electronic) 951-22-8182-1

Publisher TKK Optoelectronics Laboratory

The dissertation can be read at http://lib.tkk.fi/Diss/2006/isbn9512281821/

VÄITÖSKIRJAN TIIVISTELMÄ

TEKNILLINEN KORKEAKOULU
PL 1000, 02015 TKK
http://www.tkk.fi

Tekijä Juha Riikonen

Väitöskirjan nimi

Itseorganisoituvat nanorenkaat ja jännityksen indusoimat kvanttipisteet

Käsikirjoituksen jättämispäivämäärä 23.1.2006	Väitöstilaisuuden ajankohta 2.6.2006
Yhdistelmäväitöskirja (yhteenveto + erillisartikkelit)	Sivumäärä 56+62

Osasto	Sähkö- ja tietoliikennetekniikan osasto
Laboratorio	Optoelektroniikan laboratorio
Tutkimusala	Nanotekniikka
Vastaväittäjä	Prof. Srinivasan Anand
Työn valvoja	Prof. Harri Lipsanen

Tiivistelmä

Tässä väitöstyössä valmistettiin ja tutkittiin itsejärjestyviä yhdistepuolijohteiden nanorakenteita. Näytteet valmistettiin metallo-orgaanisella kaasufaasiepitaktisella (engl. metalorganic vapor phase epitaxy, MOVPE) menetelmällä. Atomivoimamikroskopiaa (engl. atomic force microscopy, AFM) käytettiin pinnan morfologian tutkimiseen. Optisia ominaisuuksia tutkittiin fotoluminesenssimittauksilla (engl. photoluminescence, PL).

Kvanttipisteitä on tyypillisesti valmistettu peittämällä itsejärjestyneitä puolijohdesaarekkeita toisella puolijohteella, jolla on saarekemateriaalia suurempi energia-aukko. Tässä työssä kvanttipisteitä kuitenkin valmistettiin pinnan läheisyydessä olevaan kvanttikaivoon saarekkeiden indusoiman jännityksen avulla (nk. jännityskvanttipisteet). Aluksi toteutettiin jännityskvanttipisteiden valmistamiseen soveltuva uusi materiaalisysteemi, jossa käytettiin InGaAs(P)/InP-kvanttikaivoa sekä InAs-saarekkeita. PL-spektrissä havaittiin selkeästi neljän jännityskvanttipistetilan maksimit. Saarekekokonaisuutta optimoitiin laskemalla lämpötilaa saarekekasvun aikana. Jännityskvanttipisteiden luminesenssiaallonpituutta säädettiin kvanttikaivon koostumusta muuttamalla. Lisäksi kvanttipisteiden ominaisuuksia muutettiin mm. valmistamalla eri kokoisia saarekkeita sekä vaihtelemalla kvanttikaivon etäisyyttä pinnasta.

Seuraavaksi työssä tutkittiin itsejärjestyvien InAs-saarekkeiden muodon muuttamista nanorenkaiksi. Aikaisemmissa tutkimuksissa muodonmuutoksessa hyödynnettiin saarekkeiden osittaista peittämistä. Tässä työssä muodonmuutos saatiin aikaan käyttämällä ainoastaan fosforilämpökäsittelyä. Muodonmuutoksen oletetaan aiheutuvan aluksi tapahtuvasta arseeniatomien vaihtumisesta fosforiatomeiksi sekä tätä seuraavasta indiumatomien uudelleen ryhmittymisestä energeettisesti edullisempiin paikkoihin.

Lopuksi tutkittiin GaAs-pinnan passivointia ohuen epitaktisen GaN-kerroksen avulla. Passivoinnin vaikutusta arvioitiin mittaamalla PL-spektrejä näytteistä, joissa InGaAs/GaAs-kvanttikaivo on pinnan läheisyydessä. Passivointikerroksen aikaansaaman PL-intensiteetin kasvun perusteella pääteltiin, että epitaktisesti valmistettu GaN-kerros on tehokas tapa passivoida GaAs-pinta.

Avainsanat MOVPE, epitaksia, nanoteknologia, itsejärjestäytyvä, yhdistepuolijohde, kvanttipiste, kvanttirengas, nanorengas, passivointi

ISBN (painettu) 951-22-8181-3	ISBN (elektroninen) 951-22-8182-1

Julkaisija TKK Optoelectroniikan laboratorio

Luettavissa verkossa osoitteessa http://lib.tkk.fi/Diss/2006/isbn9512281821/

Preface

The work presented in this thesis has been carried out at the Optoelectronics Laboratory of Helsinki University of Technology during 2000 – 2005. I want to express my gratitude to Professor Turkka Tuomi and Professor Harri Lipsanen for giving me the opportunity to work at the laboratory and for their continuous support during this time.

I like to thank Docent Markku Sopanen for guidance and advice. I am deeply indebted to him for his help. I would also like to thank my collaborator Doctor Jaakko Sormunen. Our cooperation has been pleasant and, moreover, productive. I thank Marco Mattila and Hannu Koskenvaara for their valuable assistance and fruitful conversations on the way. All the personnel in Optoelectronics laboratory I want to thank for the enjoyable atmosphere.

The financial support of the Graduate School of Electronics Manufacturing is gratefully acknowledged.

I thank my parents for encouragement and support throughout the journey, and sisters Jaana and Johanna for putting up with me all these years. Finally, I want to thank my loving wife Tanja and delightful daughter Enni — You are my inspiration.

"It is quite probable that other new physical principles will also be utilized to practical ends as the art develops."

— WILLIAM SHOCKLEY in his Nobel Lecture, December 11, 1956.

Espoo, May 2006

Juha Riikonen

Table of Contents

Preface . . . vii

Table of Contents . . . viii

List of Publications . . . x

Author's contribution . . . xi

1 Introduction **1**

2 Experimental methods **4**

2.1 Metalorganic vapor phase epitaxy . . . 4

2.2 Atomic force microscopy . . . 6

2.3 Optical spectroscopy . . . 7

3 III-V semiconductor nanostructures: an introduction **9**

3.1 Fabrication . . . 9

3.2 Strain-induced quantum dots by self-assembled growth . . . 11

3.3 Self-assembled nanorings . . . 15

4 Experimental results and discussion **18**

4.1 Strain-induced InGaAs(P)/InP quantum dots . . . 18

4.1.1 Demonstration of self-assembled InAs stressors islands 18

4.1.2 Modification and tunability 20
4.1.3 Time-resolved optical properties 25
4.2 InAs nanorings on InP 29
4.2.1 Fabrication of self-assembled nanorings 29
4.2.2 Island-to-ring evolution 31
4.3 GaN passivation of GaAs surface 33

5 Summary **38**

References **40**

List of Publications

This thesis consists of an overview and of the following publications:

I J. Riikonen, J. Sormunen, M. Mattila, M. Sopanen, and H. Lipsanen, *InGaAs/InP quantum dots induced by self-organized InAs stressor-islands*, Japanese Journal of Applied Physics **44**, L518–L520 (2005).

II J. Sormunen, J. Riikonen, M. Mattila, M. Sopanen, and H. Lipsanen, *Modified self-assembly of InAs islands acting as stressors for strain-induced InGaAs(P)/InP quantum dots*, Nanotechnology **16**, 1630–1635 (2005).

III J. Riikonen, J. Sormunen, H. Koskenvaara, M. Mattila, M. Sopanen, and H. Lipsanen, *Highly tunable emission from strain-induced InGaAsP/InP quantum dots*, Japanese Journal of Applied Physics **44**, L976–L978 (2005).

IV H. Koskenvaara, J. Riikonen, J. Sormunen, M. Sopanen, and H. Lipsanen, *Carrier dynamics in strain-induced InGaAsP/InP quantum dots*, accepted for publication in Physica E.

V J. Riikonen, J. Sormunen, H. Koskenvaara, M. Mattila, A. Aierken, T. Hakkarainen, M. Sopanen, and H. Lipsanen, *Effect of surface states on carrier dynamics in InGaAsP/InP stressor quantum dots*, Nanotechnology **17**, 2181–2186 (2006).

VI J. Sormunen, J. Riikonen, M. Mattila, J. Tiilikainen, M. Sopanen, and H. Lipsanen, *Transformation of self-assembled InAs/InP quantum dots into quantum rings without capping*, Nano Letters **5**, 1541–1543 (2005).

VII J. Sormunen, J. Riikonen, T. Hakkarainen, M. Sopanen, and H. Lipsanen, *Evolution of self-assembled InAs/InP islands into quantum rings*, Japanese Journal of Applied Physics **44**, L1323–L1325 (2005).

VIII J. Sormunen, J. Riikonen, M. Sopanen, and H. Lipsanen, *GaN/GaAs(100) superlattices grown by metalorganic vapor phase epitaxy using dimethylhydrazine precursor*, Journal of Crystal Growth **270**, 346–350 (2004).

IX J. Riikonen, J. Sormunen, H. Koskenvaara, M. Mattila, M. Sopanen, and H. Lipsanen, *Passivation of GaAs surface by ultrathin epitaxial GaN layer*, Journal of Crystal Growth **272**, 621–626 (2004).

Author's contribution

For all of the publications, the sample structures and experiments were planned by the author and the co-authors.

The author and J. Sormunen have fabricated the samples for publications I, II, III, IV, V, VIII, and IX. For publications VI and VII samples were grown by J. Sormunen.

Photoluminescence measurements for publications I, II, III, VI, and IX were performed by the author. For publication V the studies were carried out by the author, A. Aierken, and H. Koskenvaara and for publication VII by J. Sormunen.

The surface morphology for publication V was analyzed by the author. For the rest of the publications, analyses were conducted by J. Sormunen.

Strain calculations have been conducted by M. Mattila and rate equation analyses have been carried out by H. Koskenvaara.

The author has written the manuscripts for publications I, III, V, and IX and has also participated in the interpretations of the results and revision of the manuscripts for the publications II, IV, VI, VII, and VIII.

1 Introduction

The usefulness of semiconductors was truly revealed upon the invention of the transistor. Since then, the semiconductor technology and its applications have evolved tremendously. For example, the mobile phones with a video call and live television were just a vague dream some years ago and without semiconductor technology there would be no Internet as we know it today. Electronic circuit miniaturization and circuit integration alongside with the extraordinary properties of semiconductors have made all of this possible.

Silicon is the standard material in electronics involving integrated circuits. However, silicon is not suitable for light emitting devices due to its fundamental physical properties. Thus, III-V compound semiconductors are predominantly used in optoelectronics for the fabrication of optically active devices such as light emitting diodes (LEDs) and lasers. Laser diodes, e.g., form the backbone of the Internet by enabling fiber optical telecommunication.

In the evolutionary process of applications, advances in device design are truly important, but the fabrication technology needs to reach a mature state, as well. The ever-ongoing development of heteroepitaxial fabrication techniques has enabled the realization of state-of-the-art compound semiconductor structures. With heteroepitaxy, two-dimensional layers or thin films can be used to fabricate a quantum well (QW) structure in order to confine charge carriers in one dimension (1D). On the other hand, to produce three-dimensional (3D) confinement, i.e., quantum dots (QDs), self-assembled semiconductor islands are typically embedded in a matrix of another semiconductor material with a higher band gap (so-called buried QDs). These kinds of structures can be used as an optically active region, e.g., in lasers.

In the pursuit of new applications, nanotechnology has recently evoked more interest. This interdisciplinary field of science focuses on, as the name im-

plies, structures on the nanometer scale. Quantum mechanics play an essential role in determining the novel characteristics of structures on this scale, e.g., carrier confinement in a QD results in an energy level quantization. In many cases, nanostructures are fabricated by exploiting the ability of nature to self-organize or self-assemble atoms and molecules. This thesis combines optoelectronics and nanotechnology, and mainly focuses on the epitaxial self-assembled islands and how they are exploited especially in the fabrication of QD structures.

Besides creating QDs by burying self-assembled islands, also strain-induced QDs (SIQDs) or stressor QDs can be fabricated. SIQDs are realized by straining a near-surface QW by self-assembled islands. The stressor islands on top of the structure induce confining enclosures, i.e., QDs, in the QW. Moreover, SIQDs present an intriguing structure in the pursuit of high optical quality QDs, because these QDs reside within a high quality QW away from the sample surface. The main focus in this thesis is in the fabrication and investigation of SIQDs. In publication I, a novel SIQD material system utilizing InGaAs/InP QW and InAs islands as stressors was demonstrated. In publications II and III, modification and tunability of InGaAs(P)/InP SIQDs were studied. Carrier dynamics of InGaAsP/InP SIQDs was investigated in publications IV and V.

While fabricating buried QDs, self-assembled islands are capped by fully overgrowing them. On the other hand, partial capping can be used to transform the morphology of the islands into volcano-like nanorings (NRs). These nanostructures present an interesting topic in nanotechnology due to the potential offered by the unique topology. Moreover, investigation of the island-to-ring transformation helps to further refine the growth of self-assembled islands especially when fabricating buried QDs. In publications VI and VII, fabrication and characteristics of self-assembled InAs nanorings on InP were studied. Instead of employing the typical approach of partial capping, a new island-to-ring transformation process without capping was demonstrated.

Disruption of the periodic semiconductor crystal lattice by the sample surface can lead to the formation of electrically active surface states, which are usually detrimental to the optical and electrical characteristics, and especially so in low-dimensional structures. Consequently, exploitation of an epitaxial ultrathin GaN layer in the passivation of a GaAs surface was also studied in this thesis. Growth of GaN on GaAs was based on the results in publication VIII and passivation by GaN was studied in publication IX.

Near-surface InGaAs/GaAs QWs were used as a low-dimensional test structures in the passivation studies.

This overview has been organized as follows. The main experimental methods used in this thesis are described in chapter 2. A short introduction to III-V compound semiconductor nanostructures within the scope of this thesis is given in chapter 3. The experimental results of this work are presented in chapter 4. More specifically, section 4.1 summarizes the work on strain-induced InGaAs(P)/InP QDs. InAs nanorings are discussed in section 4.2. Section 4.3 presents results on the GaN passivation of a GaAs surface. Finally, the main results of this thesis are summarized in chapter 5.

2 Experimental methods

The experimental techniques essential to this thesis are introduced in this chapter. The sample fabrication by metalorganic vapor phase epitaxy (MOVPE) is explained in section 2.1. Section 2.2 presents atomic force microscopy (AFM) used to characterize the surface morphology of the samples. Optical spectroscopy measurements are outlined in section 2.3.

2.1 Metalorganic vapor phase epitaxy

MOVPE is a method of chemical vapor deposition for the epitaxial growth of materials utilizing the pyrolysis of metalorganic compounds. In epitaxial growth, the crystalline structure of the substrate is reproduced or mimed to the deposited layer. More specifically, it is called homoepitaxy if the substrate and the deposited material are the same. Term heteroepitaxy, on the other hand, is used when one material is grown on another (e.g. InGaAs on InP). The MOVPE process or apparatus is also referred to as organometallic vapor phase epitaxy (OMVPE), organometallic chemical vapor deposition (OMCVD), and metalorganic chemical vapor deposition (MOCVD). The term MOVPE is used throughout this thesis.

In general, chemical vapor deposition (CVD) results from chemical reactions of precursors in the vicinity of the substrate typically at temperatures between 500 and 1100 °C. MOVPE is a specific CVD process, which utilizes metalorganic compounds as precursors and it is especially suitable for the fabrication of semiconductor single crystals. MOVPE enables, e.g., the fabrication of highly homogeneous layers, atomically flat surfaces, and sharp interfaces in heteroepitaxy while controlling the composition precisely. In order to gain reproducibility, computers are typically used to control the MOVPE systems during the growth process.

The semiconductor structures studied in this thesis were fabricated by a MOVPE system manufactured by Thomas Swan Scientific Equipment Ltd. The main parts of the MOVPE: the gas system, reactor, and gas exhaust and cleaning are shown schematically in Fig. 2.1. The metalorganic precursors are in steel containers known as bubblers. Carrier gas, in this case hydrogen, is used to transport the metalorganic compounds. The concentration of metalorganics in the carrier gas is determined by the vapor pressure of the precursor, which can be controlled by adjusting the precursor temperature. In order to provide a stable concentration of metalorganics, the bubblers are located in temperature controlled baths. Metalorganics used in this thesis were trimethylgallium (TMGa), trimethylindium (TMIn), tertiarybutylphosphine (TBP), tertiarybutylarsine (TBAs), and dimethylhydrazine (DMHy).

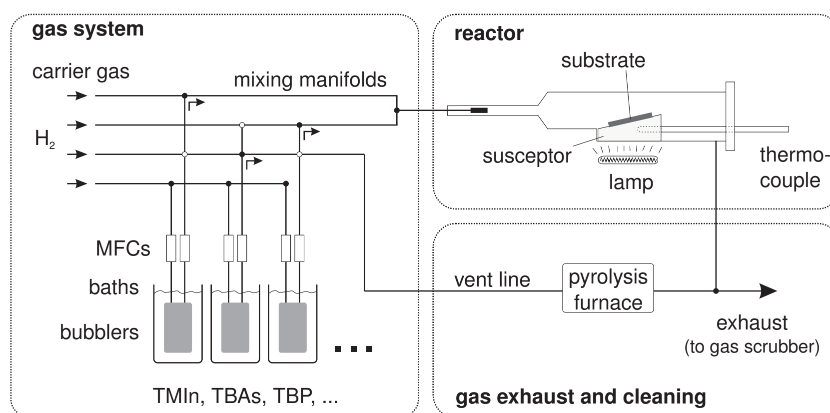

Figure 2.1. Schematic diagram of the MOVPE system.

The flow rate of the gas is controlled by mass flow controllers (MFCs) throughout the system. Mixing manifolds are used to direct the metalorganic compounds to the reactor whereas the vent line is used to flush the gas directly to the exhaust. For example, while growing an InP layer, TMIn and TBP are lead to the reactor while the rest of the organometallics are directed to the vent line, as indicated in Fig. 2.1. All the exhaust gases from the reactor and the vent line are finally absorbed and oxidized in a scrubber.

The epitaxial growth takes place in the horizontal quartz-glass reactor where the substrate is placed on a graphite susceptor. The maximum size of the substrate is $2{\times}2$ cm^2. The susceptor is heated by a halogen lamp, which is located outside the reactor underneath the susceptor, as depicted in Fig. 2.1.

The temperature is measured by a thermocouple inside the susceptor. It should be noted that the gas flow cools the substrate. In a similar reactor, when the thermocouple reading is 650 °C the actual temperature at the sample surface is approximately 50 °C lower [1]. All the temperatures mentioned in this thesis are thermocouple readings.

The samples in this thesis were fabricated on semi-insulating InP(001) and GaAs(001) substrates at atmospheric pressure. Prior to the growth process the substrates were annealed at 650–700 °C in the reactor to remove the native oxide. The temperature in the growth process was typically between 540 and 640 °C whereas the growth rate was around 0.3 nm/s. Detailed information about the growth procedures can be found in section 4 of this overview and in the publications of this thesis.

2.2 Atomic force microscopy

Atomic force microscopy was invented by Binning *et al.* in 1986 [2]. They described the atomic force microscope as a combination of the principles of the scanning tunneling microscope (STM) and the stylus profilometer. As depicted in Fig. 2.2, the basic principle of the AFM is quite simple. A sharp tip, typically composed of silicon or silicon nitride, on a cantilever is brought into a close proximity of the surface. At the same time, a laser beam is used to detect the deflection of the cantilever caused by an electrostatic force between the tip and the sample. Feedback is used to keep the force, i.e., the distance, between the tip and the sample constant. This is done by moving the sample or tip vertically using piezoelectric actuators. In order to scan a map of the surface features, similar actuators are used to move the sample or tip in lateral directions. The AFM technique achieves a high magnification of the surface features in all three dimensions contrary to optical or electron microscopes (which provide a two-dimensional (2D) projection of the surface). Moreover, AFM is rather versatile since the measurement can be carried out in ambient air and the samples do not need any special preparation. It can be also used to measure conducting as well as insulating samples.

The maximum scan area of the contact-mode NanoScope E AFM utilized in this thesis is 13×13 μm^2. Nominal radius of the non-conductive silicon nitride tips used is 10 nm. In detailed analysis, the finite curvature of the tip should be taken into consideration, since the scanned image is a convolution of the tip and the surface profile. In this thesis, AFM is mainly used to study

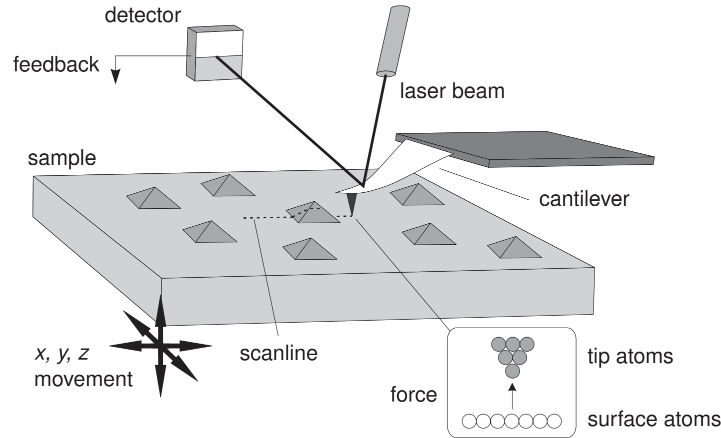

Figure 2.2. A schematic illustration of atomic force microscopy.

the areal density and the size of self-assembled InAs islands. Because the number of the islands in the maximum scan area is typically around 2000 and the size of the islands needs not to be determined to extreme precision, these shortcomings do not play a significant role.

2.3 Optical spectroscopy

The optical properties of the samples investigated in this thesis were studied by photoluminescence (PL) measurements. The term photoluminescence is used when light is utilized for excitation in order to gain luminescence from a substance. Electron–hole pairs created in photon absorption thermalize rapidly to the band edge and then the carriers move by diffusion and drift. In a semiconductor structure with a QW, for example, the carriers are easily transported to the QW region. Before recombination, free carriers are mostly relaxed to the ground state of the QW. Information about the energy level structure [publications I–IX] and the carrier dynamics [publications III, IV, V] of the samples can be gatherer by studying the emission spectra and the temporal behavior of the PL, respectively.

In this thesis, the optical properties of the samples were studied by low-temperature (10 K) continuous-wave photoluminescence (cw-PL) and time-resolved photoluminescence. The setup used for the cw-PL is shown in Fig. 2.3 (a). The samples were cooled in a closed-cycle helium cryostat. In

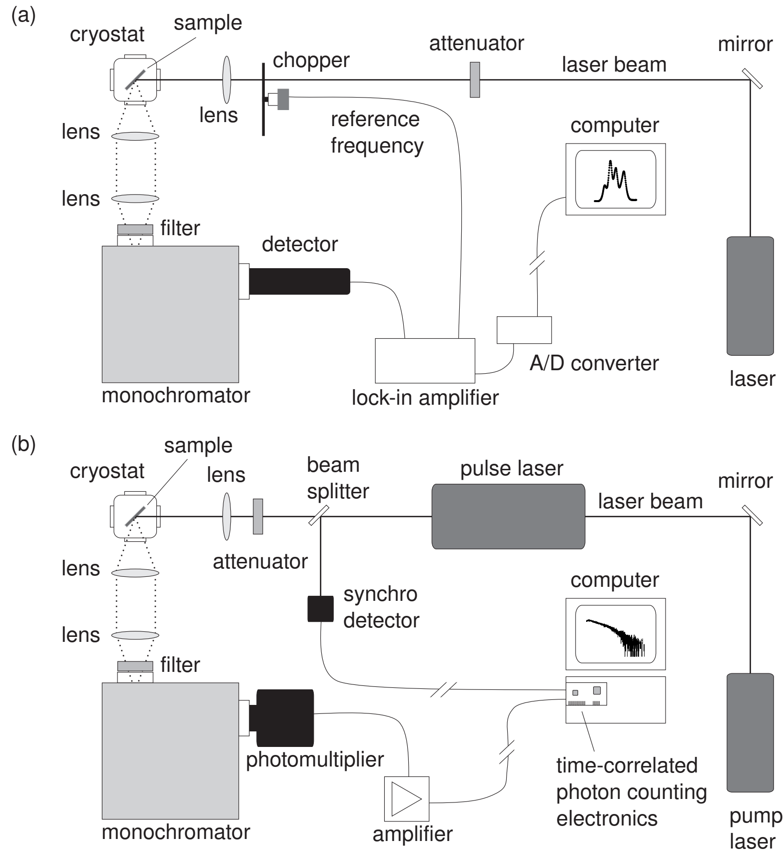

Figure 2.3. Schematic diagram of (a) the continuous-wave PL and (b) time-resolved PL setup.

the cw-PL measurements a frequency-doubled Nd:YVO_4 laser operating at 532 nm was used for excitation. In publication IX, however, a 488 nm line from an argon-ion laser was used for optical excitation. The PL spectra were recorded using a 0.5 m monochromator with a germanium detector cooled to liquid nitrogen temperature while utilizing a lock-in amplifier.

The TRPL measurements were performed by exciting the samples with 150-fs pulses at 800 nm from a mode-locked Ti:sapphire laser with a repetition rate of 76 MHz (Fig. 2.3 (b)). The laser used in cw-PL was used as a pump-laser for the Ti:sapphire laser. The PL transients at selected wavelengths were detected by a Peltier-cooled microchannel plate photomultiplier and time-correlated single photon counting electronics. The temporal resolution of the system was approximately 30 ps.

3 III-V semiconductor nanostructures: an introduction

This chapter gives a brief introduction to semiconductor nanostructures. Fabrication is outlined briefly in section 3.1. Strain-induced quantum dots are introduced in section 3.2 whereas self-assembled nanorings are discussed in section 3.3.

3.1 Fabrication

Nanostructure is quite commonly defined in semiconductor physics as a structure with two or three dimensions in the nanometer scale. When the movement of the carrier is restricted sufficiently at least in one dimension, quantum confinement or quantization can be achieved. More specifically, the size of the confinement needs to be comparable to the Bohr exciton radius. As a rule of thumb, for typical III-V semiconductors the transition to strong confinement occurs when the dimension is around 10 nm [3]. In a quantum well structure, electrons and holes are confined in 1D. On the other hand, in quantum wires and quantum dots, the confinement potential is in 2D and 3D, respectively. A quantum well is typically fabricated by embedding or sandwiching a thin layer of low band gap material in a high band gap material. Quantum dots, on the other hand, can be created by burying 3D nanoscale structures in a matrix of another semiconductor having a larger band gap. Typical QD fabrication techniques are described in the following section.

Basically, the different ways to create semiconductor nanostructures (and structures in general) can be divided into two classes. Despite the different approach of these techniques, they are mainly considered as complementary methods in device fabrication. One class of methods is called *top-down*

techniques. These methods are used to create structures by removing (or *carving*) material and can, e.g., involve electron beam (e-beam) lithography and etching processes. *Top-down* techniques are especially suitable in fabricating microstructures such as cantilevers for microelectromechanical systems (MEMS) or finalizing device structures of laser diodes. Another class of methods is called *bottom-up* techniques. These methods utilize self-assembled or self-organized growth in order to generate structural organization of atoms. Self-assembled nanostructures can be fabricated, e.g., by heteroepitaxy as has been done in this thesis.

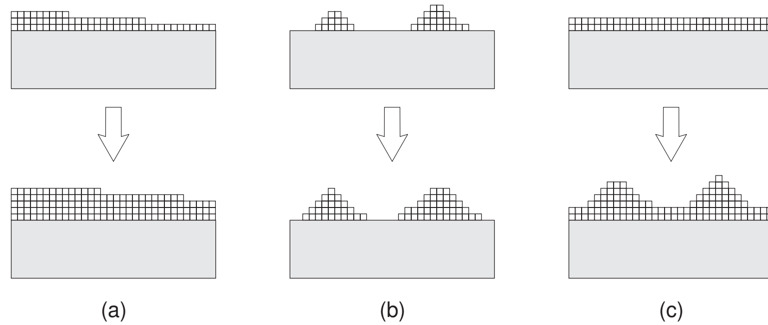

Figure 3.1. The basic growth modes in heteroepitaxy are (a) Frank-van der Merwe, (b) Volmer-Weber, and (c) Stranski-Krastanow.

The three fundamentally different growth modes in heteroepitaxy are shown schematically in Fig. 3.1. The layer-by-layer growth, shown in (a), is called the Frank-van der Merwe growth mode [4]. This 2D layer growth can be used to fabricate two-dimensional layer structures, e.g., QWs. However, the pseudomorphic strain between the layers sets a limitation to the maximum thickness. Beyond this so-called critical thickness the strained layer relaxes by generating misfit dislocations.

In the Volmer-Weber growth [5], on the other hand, the deposited atoms form 3D islands directly on the surface, as depicted in Fig. 3.1 (b). The Stranski-Krastanow growth mode [6], shown in (c), is initiated by 2D layer growth. It is typically referred to as wetting layer. However, as the critical thickness (typically few monolayers, MLs) is achieved, island formation begins. An important aspect in the self-assembled Stranski-Krastanow (S-K) growth mode is that it can be used to fabricate non-dislocated, i.e., coherently strained islands [7]. As a result, islands grown by the so-called coherent S-K growth can be used in optically active structures.

3.2 Strain-induced quantum dots by self-assembled growth

The common way to fabricate QDs is to bury self-assembled islands in a matrix of another semiconductor having a larger band gap, shown schematically in Fig. 3.2 (a). Alternatively, a QD can also be realized by using a QW structure as a starting point and introducing the lateral confinement by other means, shown in Figs. 3.2 (b) – (d).

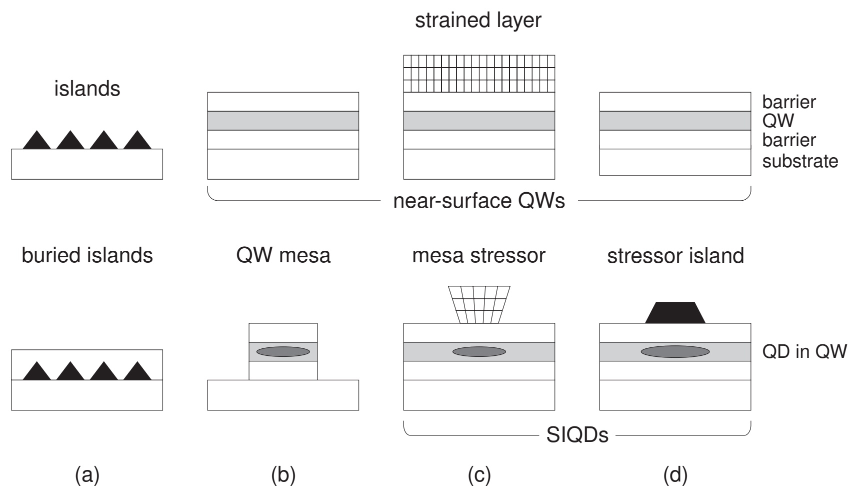

Figure 3.2. QDs created utilizing (a) buried islands, (b) etched QW mesa, (c) SIQD by strained mesa, and (d) SIQD by self-assembled stressor islands. The QD is formed (a) in the islands themselves and (b) – (d) in the near-surface QW.

Using the *top-down* approach, as depicted in (b), an etched mesa can be used to create lateral confinement in the planar QW structure [8, 9]. In this structure, however, the large etched surface with crystal defects created in the etching process can be detrimental to the quantum efficiency of light emission. A more sophisticated approach is to grow a pseudomorphic compressively strained layer on top of a near-surface QW structure [10]. The etched mesa of the strained layer, called a stressor, creates local strain underneath the stressor, which effectively creates a strain-induced QD inside the near-surface QW as depicted in (c). These were the first strain-induced QDs reported. However, the critical thickness of the strained layer limits

the maximum strain. As a consequence, the achieved confinement is quite weak. All in all, the *top-down* methods do not usually provide viable means to create high quality QD structures.

As shown in Fig. 3.2 (d), self-assembled islands grown on top of the capping layer of the near-surface QW structure can also be utilized as stressors to create strain-induced QDs into a near-surface QW. With this method, first demonstrated by Sopanen *et al.* [11], the structure can be fabricated *in situ* with a single growth run requiring no additional processing steps. While fabricating QDs utilizing QW mesa or mesa stressor structures, e.g, by e-beam lithography, the lateral position of the QDs can be determined exactly. This cannot be done in self-assembled growth, and it is not even necessary in typical optoelectronic applications. More importantly, the size, shape, and areal density of the nanostructures can be varied in self-assembled growth. In the e-beam technique, the structures are patterned one by one whereas by self-assembled growth, islands with an areal density of around 10^9 cm^{-2} can be fabricated even on several wafers in one growth run. Moreover, the coherent self-assembled islands induce larger strain on the QW underneath, which results in a deeper confinement potential. More specifically, as shown in Fig. 3.3 (a), the tensile strain reduces the band gap of the material underneath the stressor island. The local deformation creates a lateral (or in-plane) confinement potential for both electrons and holes. The vertical confinement, on the other hand, is achieved by the high-quality interfaces of the QW. As a result, the SIQD is formed into a strain-modified region of the QW.

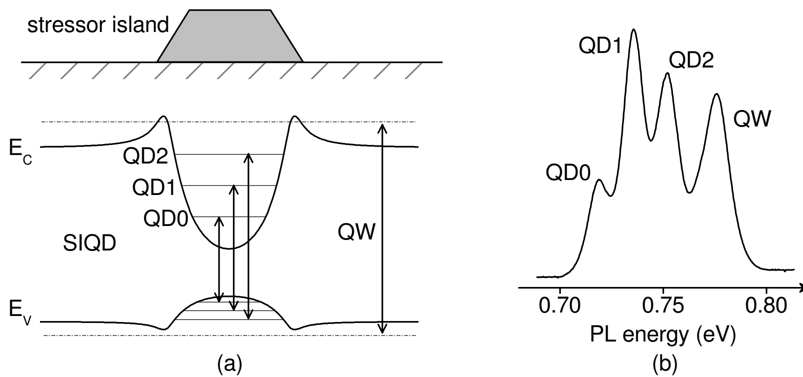

Figure 3.3. (a) Schematic illustration of the in-plane confinement potential and (b) a typical SIQD PL spectrum of the SIQD.

Fig. 3.3 (b) shows a typical SIQD PL spectrum [publication III]. The PL peaks corresponding to QD ground state along with the first and second excited states are labeled with QD0, QD1 and QD2, respectively. To understand the observed PL behavior, carrier relaxation and recombination processes are briefly discussed based on the studies of InGaAs/GaAs SIQDs [12]. Carriers created by excitation are directed by the funnel-like potential[1] toward the SIQDs [13]. Then, the carriers relax either straight into the SIQD or to the QW, from which they are mainly recombined radiatively or captured into the SIQD (referred to as QD capture). The QD capture process is mediated by Coulomb scattering and longitudinal optical phonon emission [14, 15]. Once captured into the SIQD, the holes and electrons can either experience relaxation to the lower energy states or recombine radiatively. Two mechanisms are reported to be responsible for the intraband relaxation of the carriers: Coulomb scattering is shown to be effective when the QW is highly populated [14] whereas an Auger-like mechanism has been reported to mediate the relaxation in a low density case [16]. This Auger-like process involves the transition of an electron to a lower level in the SIQD, while a hole is ejected into the QW.

A review of the SIQDs by Lipsanen *et al.* [12] says that "the most prominent feature in the optical properties of the stressor QDs is the intense luminescence from the excited states due to state filling". This sums up the essence of the SIQDs. In InGaAs/GaAs SIQDs, intraband relaxation has been shown to be a faster process (time constant $\tau < 10^{-9}$ s) than optical recombination ($\tau \sim 10^{-9}$ s) [16, 17]. Accordingly, only the luminescence from the ground state of the SIQD is expected to be seen when applying low excitation intensities in the PL measurements. However, as the excitation intensity is increased, state filling may occur, i.e., a nearly filled state prohibits relaxation from a higher state (Pauli blocking) and the next level starts to populate [17, 18]. Thus, with increasing excitation intensity, the luminescence from consecutive energy levels can be seen to emerge. Eventually, luminescence from all of the QD energy states can be observed in the PL spectrum (as in Fig. 3.3 (b)).

Because of the clearly resolved PL peaks, cw-PL and time-resolved PL (TRPL) have enabled the detailed study of the characteristics of these quantum dots [14, 17–19]. Carrier dynamics in SIQDs has been further analyzed by the rate equation model [17] and master equations [16, 20]. SIQDs are also an ideal model system for fundamental investigations of QDs, especially as the strain and the induced nearly-parabolic confinement potential can be modeled in a straightforward manner [13, 14, 17, 18]. A cylindrical

[1] The directing potential is also created by the strain of the stressor island.

symmetry has been assumed in these calculations using a ΔT finite element method (ΔT FEM). The same method was also used in the computation in publications II, III, and V. Since the confinement potential is determined by the stressor-induced strain, the energy levels can be tailored by modifying the structural parameters of the SIQD [21].

Although most of the studies have been done on InGaAs/GaAs SIQDs created by InP stressors [12], GaInNAs/GaAs [22], GaInP/AlGaInP [23], GaAs/AlGaAs [24, 25], and SiGe/Si [26] QWs have also been used to fabricate SIQDs. For reference, the band gaps of some III-V compound semiconductors are shown as a function of lattice constant in Fig. 3.4.

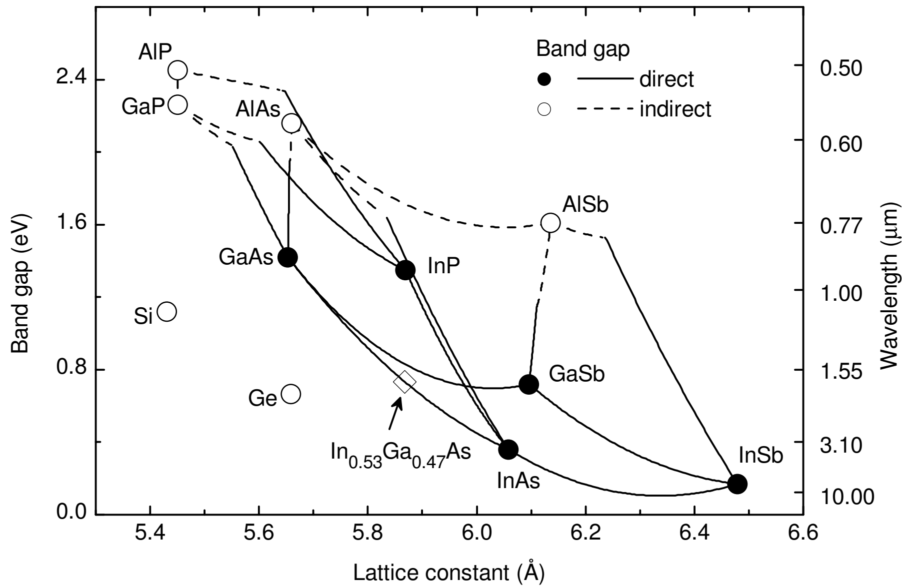

Figure 3.4. Band gaps of some III-V compound semiconductors as a function of lattice constant. Solid lines and filled circles correspond to direct band gap whereas dashed lines and open circles mark indirect band gap.

Besides InP islands, also GaSb [25], Ge [26] and InAs [27] islands have been utilized as stressors. However, InP is a quite suitable stressor material for the GaAs-based systems since the lattice mismatch of InP/GaAs (3.8 %) allows coherent islands up to about 120 nm in diameter and, in addition, InP passivates the GaAs surface, thus reducing surface recombination [11, 19, 28, 29]. In the case of GaSb stressor islands, on the other hand, surface recombination is found to significantly diminish the PL intensity of

the QDs [25, 29]. GaSb has a lower band gap (0.81 eV) compared to that of InP (1.34 eV) and GaAs (1.42 eV). Additionally, the strain induced by the GaSb stressors reduce the QW barrier. These have reported to explain the enhanced surface recombination [29] (despite that the GaSb/GaAs heterojunction has band alignment of type-II [30]). Moreover, due to the large lattice mismatch of GaSb/GaAs (7.8 %), the optimum (maximum) diameter for coherent GaSb stressors is only 36 nm [29]. Therefore, the achieved depth of the confinement potential is quite small. For InP stressors, the energy separation (redshift) between the QD0 and QW states determined from PL spectra is 105 meV [18] whereas a separation of only 21 meV has been reported for GaSb stressors [29].

A new material system was introduced to fabricate SIQDs in this work. InGaAs(P)/InP SIQDs utilizing InAs stressor islands were studied in publications I-V. As indicated in Fig. 3.4, the use of InP substrate instead of GaAs allows lattice-matched InGaAs to be utilized in the QW. Moreover, the InP-based system would enable the use of quaternary InGaAsP, providing further tuning possibilities since the lattice constant and band gap could be varied independently. The luminescence wavelength from this system is expected to be around 1.5 µm whereas in InGaAs/GaAs SIQDs it is ∼1.0 µm. For InP substrates, InAs seems to be a good choice for stressor material since the lattice mismatch of InAs/InP (3.2 %) is roughly the same as in the case of InP/GaAs, thus allowing growth of large coherent islands. Therefore, rather large strain can be induced in the near-surface QW, which is crucial in order to create a QD with a deep confinement potential. However, due to the low band gap of InAs (0.35 eV), some surface recombination might be expected as in the case of GaSb stressors on GaAs.

3.3 Self-assembled nanorings

Due to their ring-like shape, quantum rings (QRs) or nanorings are an interesting topic for investigations because of potential applications involving magnetic flux. By placing a NR in a perpendicular magnetic field, a phase shift proportional to the flux quanta has been detected [31] (so-called Aharonov-Bohm effect [32]). Experimental observation of persistent current [33] along with optical emission from a charge-tunable NR [34] and magneto-optical behavior have also been reported [35]. Moreover, a NR laser structure has been fabricated by stacking layers of InGaAs/GaAs nanorings [36]. Theoretical studies on the properties and tunability of nanorings have also been done in order to understand and predict their characteristics [37–39].

Although some self-assembled NRs can be grown directly by a epitaxial deposition (e.g., CdTe/ZnTe [40] and GaSb/GaAs [41]), NRs are typically realized by first growing self-assembled islands and transforming them into rings utilizing a subsequent process. InAs NRs on GaAs have been created by a so-called partial capping layer technique as follows. After the growth of InAs islands on GaAs, a thin GaAs capping layer is deposited to partially cover the islands. It is important that the islands are not fully covered. The island-to-ring transformation is achieved by annealing the partially capped islands in an As ambient, e.g., 1 min at 530 °C [42]. Finally, the sample is cooled down to room temperature for further investigations.

The transformation of an island into a nanoring has been described as *a nanoscopic volcano eruption* [43]. Two different models have been suggested to explain the transformation process [44]. A kinetic model is based on the different surface diffusion rates of group III atoms. More specifically, In atoms, which are more mobile at typical annealing temperatures, diffuse outward and leave a void at the initial location of the InAs island. Furthermore, the diffused In atoms experience In-Ga alloying resulting in an immobile InGaAs at the outer rim, which together with the void form the ring-shaped nanostructure [42, 43, 45].

A thermodynamic model, on the other hand, suggests that the cap layer induces a change in the balance of surface free energy and, consequently, an outward pointing force is created [42, 46]. As a result, the system finds an equilibrium in a nanoring structure via material redistribution. However, it has been concluded that the formation of the rings is promoted by both kinetic and thermodynamic mechanisms [42].

Furthermore, the formation of SiGe/Si NRs [47] by partial capping layer has been explained by island strain distribution. In that case, Si from partial capping layer deposition diffuses outwards from the top of the Ge island. Simultaneously through surface segregation and diffusion, Ge atoms are released from the island. They mix and alloy with Si on the island side surface where the lateral lattice constant matches SiGe with varying composition.

It has been also shown that the chemical potential of partially relaxed, coherent InAs/GaAs islands causes Ga adatom migration away from the island top surface [48]. Moreover, strain-driven In migration away from the partially capped InAs/InP islands has been shown to result in a modification of the island morphology, even holes [49]. Furthermore, it has been reported that under arsenic overpressure, In atoms tend to migrate from a strained InP surface toward the apex of InAs islands [50].

Besides the characterization and exploitation of the novel properties of nanorings, the fundamental study of NR fabrication comprises unanswered issues as shortly reviewed above. Moreover, investigating the island-to-ring transformation process relates also to understanding the mechanisms involved in the fabrication of QD structures, e.g., while growing a matrix of buried QDs for a laser structure.

Transformation of self-assembled InAs/InP islands to nanorings utilizing only phosphorous annealing was studied in publications VI and VII. Since self-assembled nanorings have previously been fabricated by utilizing partial capping, this novel fabrication method can contribute to the understanding of the island-to-ring transformation mechanisms. The fact that the separated transformation process does not virtually set any requirements or limitations regarding the cap layer can be capitalized while exploring these nanorings.

4 Experimental results and discussion

This chapter discusses the results of the publications of this thesis. The work on the InGaAs(P)/InP strain-induced quantum dots from publications I–V are presented in section 4.1. The main results of the InAs/InP nanorings from publications VI and VII are reviewed in section 4.2. Finally, section 4.3 describes the results from publications VIII and IX on the epitaxial growth of GaN on GaAs mainly focusing on the passivation of GaAs surface by GaN.

4.1 Strain-induced InGaAs(P)/InP quantum dots

4.1.1 Demonstration of self-assembled InAs stressors islands

As described in section 3.2, self-assembled islands can be used as stressors in strain-induced QD structures. Previously, InP, GaSb, and Ge islands have been used as stressors. In publication I, the use of InAs islands as stressors was introduced. The optimization of InAs islands growth was reported in publication II and is described in section 4.1.2 of this overview.

The structure used in publication I to demonstrate the feasibility of InAs stressors consisted of a near-surface InGaAs/InP QW, on which the self-assembled InAs islands were grown. The samples were fabricated by MOVPE at atmospheric pressure. Semi-insulating InP(001) substrates were first annealed at 650 °C for 5 minutes before the growth of a 100-nm InP buffer layer at 640 °C. Next, a 10-nm-thick $In_{0.53}Ga_{0.47}As$ QW was deposited, followed by a 7-nm InP barrier layer. For the growth of the InAs

islands the temperature was decreased to 560 °C. The nominal thickness of the deposited InAs was 0.8 monolayers. The schematic structure of the SIQD sample is shown in Fig. 4.1 (a).

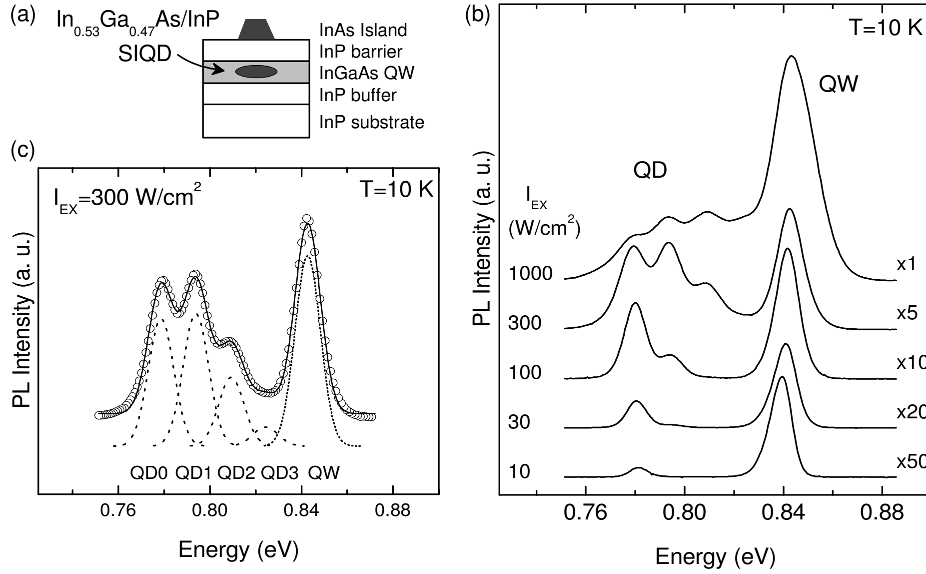

Figure 4.1. (a) Schematic SIQD structure, (b) PL spectra of the SIQD sample with varying excitation intensity, and (c) Gaussian peaks fitted to the PL spectrum.

Fig. 4.1 (b) shows PL spectra of the SIQD sample measured at 10 K using various excitation intensities. The spectrum measured at the excitation intensity of 10 W/cm^2 (lowest spectrum) shows the QD ground state peak at 0.78 eV (redshifted by 64 meV from the QW peak at 0.84 eV). As the excitation intensity is increased, the spectra clearly show at first two and then three QD peaks. Also fourth QD peak is present when the excitation is 300 W/cm^2 and above. The PL intensity of the QW peak is notably increased when the excitation is increased to 1000 W/cm^2, since all the four QD states are filled and excess carriers recombine mostly in the QW.

As shown in Fig. 4.1 (c), Gaussian peaks were fitted to the PL spectrum measured with the excitation intensity of 300 W/cm^2. It is observed that at this excitation level the third excited state has just begun to populate. The ground state along with the first, second and third excited states are labeled with QD0, QD1, QD2, and QD3, respectively. The almost equal level spacing between the energy states ($\sim$15 meV) is due to the nearly-

parabolic confinement potential. These fitted QD peaks have the same full width at half maximum (FWHM) of 13 meV as the QW peak. In studies of InGaAs/GaAs SIQDs, it has also been observed that the FWHM of the SIQD peaks and the QW peak is about the same [18]. Since no broadening due to lateral confinement inhomogeneity can be extracted (from the so-called ensemble measurement), the vertical confinement in the QW seems to determine the FWHM of the SIQD peaks. This implies that the SIQD ensemble is rather homogeneous. All in all, the results in publication I showed distinct evidence of the SIQD confinement.

The morphology of the InAs islands was characterized using a contact-mode atomic force microscope. A typical AFM image and height histogram of the islands utilized as stressors are shown in Figs. 4.2 (a) and (b), respectively. The areal density of the islands in the SIQD samples was around 10^9 cm^{-2} and the typical base diameter and height of the islands were approximately 100 nm and 22 nm, respectively.

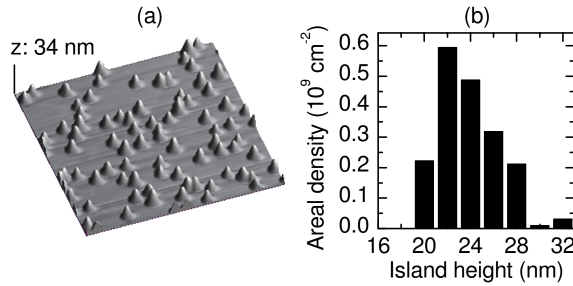

Figure 4.2. (a) Typical atomic force micrograph (2×2 μm^2) and (b) height histogram of InAs islands on top of a near-surface QW.

4.1.2 Modification and tunability

The modification of self-assembled InAs stressor islands used in strain-induced $In_{0.59}Ga_{0.41}As$/InP SIQD structure was investigated in publication II. A temperature ramp-down during the growth of the islands was utilized in order to suppress the effects of arsenic-to-phosphorus (As/P) exchange[1] [49, 51, 52]. One such undesired effect is the uncontrolled accumulation of excess material into the islands. The size and areal density of

[1] The impact of the As/P exchange is shown also in section 4.2, in which the experimental results of InAs/InP nanoring fabrication are discussed.

the stressor islands were adjusted by varying the nominal deposition thickness and the growth temperature.

Two different temperature control schemes (temperature ramp-down and constant temperature) were compared in the fabrication of InAs stressor islands. First, the temperature (550 °C) was ramped down after the growth of the InP top barrier, and the InAs islands were deposited during the first few seconds of the ramp-down. For reference, SIQD samples with the same nominal InAs deposition were fabricated at a constant growth temperature of 550 °C. After the deposition of the islands, the samples were cooled down in a TBAs flow. It was noted that although the island densities were approximately the same, the average island size was smaller in samples grown with the temperature ramp-down. As the nominal deposition thickness was the same, the variation between the samples must originate from the different temperature control procedures. Since after the InAs deposition only TBAs was directed into the reactor, As/P exchange is the most conceivable explanation for the accumulation of excess material into the islands. This implies that the temperature ramp-down has diminished the As/P exchange. Temperature ramp-down process was also observed to improve the homogeneity of the island ensemble. As a result, the temperature ramp-down was used in the fabrication of stressor islands. The growth temperatures of the islands mentioned in this thesis refer to temperatures before the ramp-down with the exception of the publication I where the stressor islands were grown at a constant temperature.

Fig. 4.3 (a) shows the areal density of InAs stressor islands plotted as a function of the average island height. Each solid line represents a different deposition thickness whereas different open symbols indicate different temperatures. The island height is seen to increase with increased temperature regardless of the nominal InAs deposition thickness. On the other hand, the density of the nucleated islands decreases with increased temperature [53]. Therefore, the same amount of deposited material is distributed over a smaller number of islands [54]. As a result, the average size of the islands is increased. This also explains the inverse relationship between the density and the average height of the islands observed in Fig. 4.3 (a). However, deposition thickness of 0.65 ML shows a different trend. Since the nominal thickness is below the critical thickness for island formation in the S-K growth [55], it was assumed in publication II that the excess material originates from the As/P exchange. In other words, the material exchange increases with temperature [51], which effectively leads to a higher nucleation density, i.e., to a higher island density.

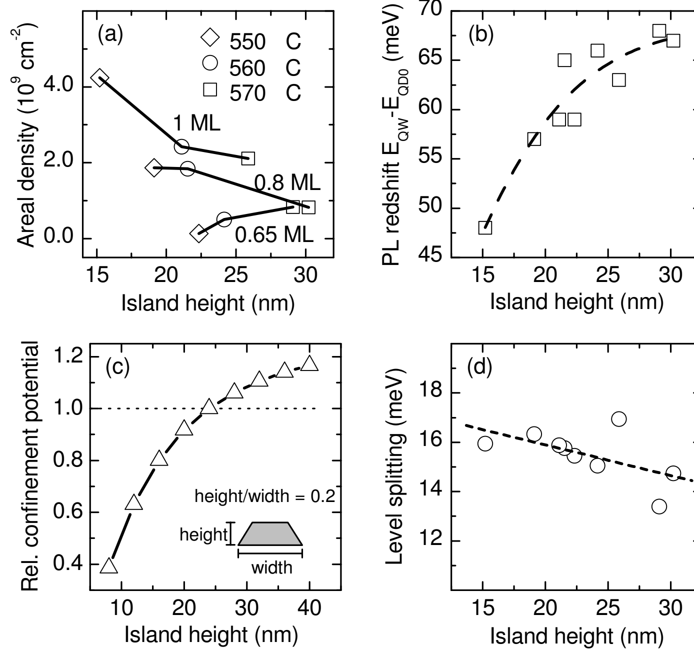

Figure 4.3. (a) Areal density of the InAs stressor islands grown with a varied temperature and InAs deposition thickness, (b) PL redshift of the QD0 peak from the QW peak, (c) calculated relative depth of the QD confinement potential (note the different height scale), and (d) average level spacing of the SIQD states as a function of the average stressor island height. The inset in (c) shows the geometry of the island used in the calculations.

The PL redshift of the QD0 peak from the QW peak is plotted as a function of the island height in Fig. 4.3 (b). As indicated by the dashed line, the initially increasing redshift starts to saturate eventually as the island size increases. Altogether, by increasing the average island height from 15 to 30 nm, the redshift increases from 47 to 67 meV. The stressor-induced strain in the center of the QW was calculated in publication II (using ΔT FEM [13] and assuming a cylindrical symmetry). The height-to-width aspect ratio of the stressor islands was fixed to 0.2 while the height of the islands was altered. In Fig. 4.3 (c) the relative depth of the confinement potential in a $In_{0.59}Ga_{0.41}As$ QW is plotted as a function of the island height (normalized to 1 at 24 nm). The calculations show a similar trend as the experimental results in Fig. 4.3 (b) (note the difference in height scales). The decreasing slope with decreasing island height implies that islands smaller than 15 nm

in height induce a rather weak confinement of carriers. On the other hand, it seems that increasing the island height above 30 nm does not increase the depth of the confinement potential significantly. Moreover, considering that increasing the island height further can result in dislocated islands, it seems that the most feasible height scale of the InAs islands for stressors is around 15 to 30 nm.

Fig. 4.3 (d) shows the average level spacing of the QD states. The QD level separation is decreased with increased island height. Increasing island size not only deepens the confinement potential but also widens it, thus explaining the reduction of the level spacing, as discussed in publication II. Typical spacing between energy states was approximately 15 meV whereas FWHM as narrow as 11 meV was observed.

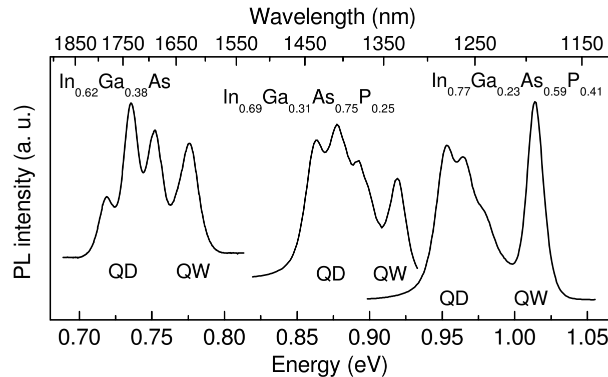

Figure 4.4. PL spectra showing the wavelength tunability of InGaAs(P)/InP SIQDs.

As shown above, the confinement potential of the SIQD can be tailored by modifying the stressor islands. In publication III, the tunability of InGaAs(P)/InP SIQD structure was studied further. First, the PL emission wavelength was tuned by varying the QW composition. Fig. 4.4 shows the PL emission between 1.3 and 1.7 µm from the SIQD InGaAs(P)/InP structure.

In publication III, the confinement potential of the QD was varied by altering the thickness of the QW and its distance from the surface. Fig. 4.5 (a) shows the calculated effect of the QW-to-surface distance, i.e., the barrier thickness, on the calculated confinement potential in the conduction band. The increasing strain in the QW along with decreasing barrier thickness is seen to result in a deeper confinement potential and higher in-plane barriers

around it. Based on the calculations, the QD0 redshift is mostly determined by the conduction band (80 – 90 %) whereas the remaining fraction originates from the heavy-hole valence band. These results are similar to the ones reported for InGaAs/GaAs SIQDs [13, 18].

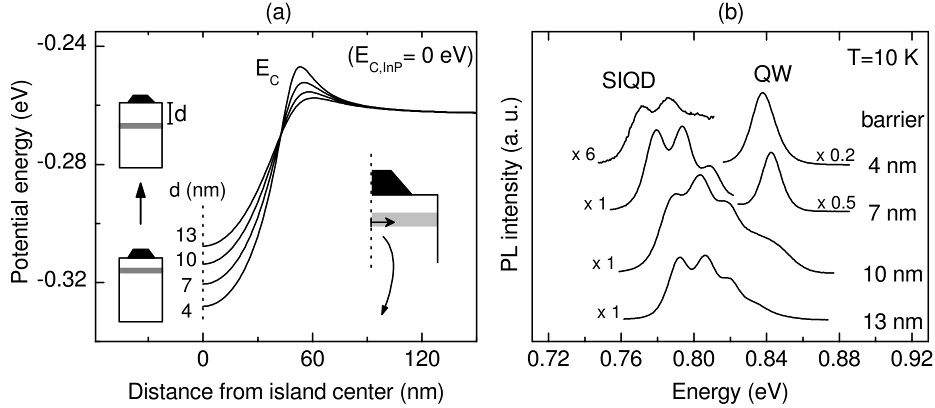

Figure 4.5. (a) The effect of barrier thickness on the confinement potential. (b) PL spectra of InGaAs/InP SIQDs with a varied barrier thickness. Curves are offset vertically and the intensity of the QW peaks in the two topmost spectra are scaled down for clarity.

Fig. 4.5 (b) shows the PL spectra of the nearly-lattice-matched InGaAs/InP SIQD samples with a varied InP barrier thickness. It can be seen that the intensity of the SIQD peak is significantly diminished when the barrier thickness is reduced from 7 to 4 nm. InAs islands are reported to have a stronger Fermi level pinning than the wetting layer, which means that the dominating surface states are related to the InAs islands [56]. Thus, it was assumed in publication III that the carriers in the proximity of InAs islands might be captured to the islands on the surface or exhibit pronounced non-radiative surface recombination.

Fig. 4.6 (a) shows the PL redshift of the QD0 peak from the QW peak as a function of the barrier thickness (determined from the PL spectra in Fig. 4.5 (b)). The redshift increases by 17 meV (to the maximum of 68 meV.) while the barrier thickness decreases from 13 to 4 nm. This is caused by increased strain, which creates a deeper confinement potential as seen in Fig. 4.5 (a). Also the effect of the QW thickness (7 – 13 nm) on the PL redshift was studied. Besides the obvious increase of the QW energy due to increased quantization ($\sim$ 30 meV, not shown here), the redshift was also observed to

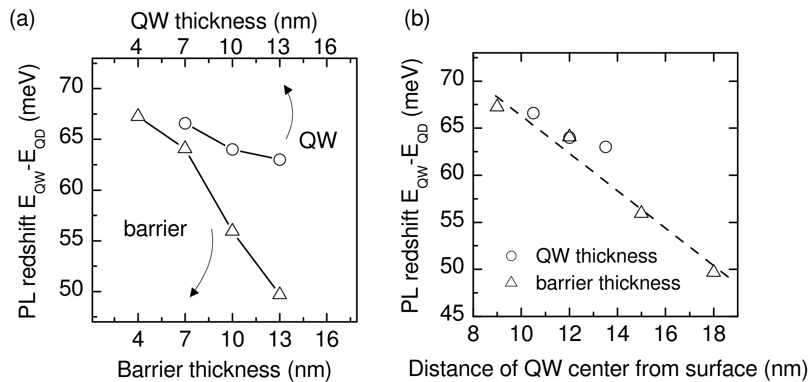

Figure 4.6. (a) PL redshift of the QD0 peak from the QW peak as a function of the barrier and QW thicknesses. (b) PL redshift plotted as a function of the distance of the QW center from the surface. The barrier and QW thickness series are plotted with triangles and circles, respectively.

increase, as shown in Fig. 4.6 (a). In Fig. 4.6 (b), the PL redshift is plotted as a function of distance from the surface to the QW center (dashed line is a guide for the eye). The results indicate that increasing the QW thickness affects the SIQD mainly by moving the center of the QW away from the surface, thus resulting in a shallower lateral confinement. This shows, as can be observed from Fig. 4.4 as well, that the QW energy does not seem to affect the redshift or the level spacing, i.e., the energy state structure of the QD significantly. In other words, the modulation of the QW band edge caused by the stressor islands is virtually independent of the vertical confinement of the QW. [publication III]

4.1.3 Time-resolved optical properties

Carrier dynamics of the InGaAsP/InP SIQDs was studied in publications IV and V in order to investigate the possible carrier capture from the SIQD to the InAs islands. The studies were conducted by time-resolved PL measurements and computational rate equation analyses. The samples consisted of InAs stressors deposited on a 10-nm-thick near-surface $In_{0.78}Ga_{0.22}As_{0.59}P_{0.41}$/InP QW. The PL intensity of the InGaAsP/InP SIQDs was seen to decrease notably with decreased barrier thickness (not

shown here). The PL spectra appeared to be similar to the PL spectra of the InGaAs/InP SIQDs in Fig. 4.5 (b).

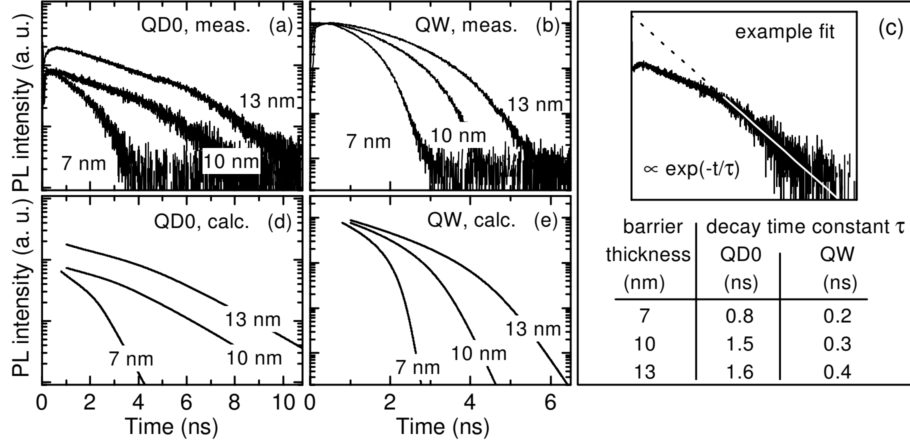

barrier thickness (nm)	QD0 (ns)	QW (ns)
7	0.8	0.2
10	1.5	0.3
13	1.6	0.4

Figure 4.7. Time-resolved PL measurements of (a) the QD0 and (b) the QW transients with a varied barrier thickness. (c) The decay time constant as determined by exponential fits showing also an example of an exponential fit. The calculated temporal behavior according to the rate equation model for (d) QD0 and (e) QW, respectively.

In Fig. 4.7 (a) the temporal behavior of the QD0 transients show decreasing slope as the barrier thickness is decreased from 13 to 7 nm. The same trend of the decreasing decay time can also be observed in the behavior of the QW transients in Fig. 4.7 (b). In Fig. 4.7 (c), the decay time constants or the effective carrier lifetimes are presented as determined by the exponential fits to the PL curves in Figs. 4.7 (a) and (b).

The TRPL measurements were also analyzed using a rate equation model. It was observed in publication IV that the typical rate equations including only the energy states of the QD [17] were not adequate. Thus, the model was amended to include the QW and the surface-related transitions. A more detailed description of the rate equations can be found in publications IV and V and references therein. All in all, the simulations were found to be in a good agreement with the experimental data showing the same trend of decreasing carrier lifetime with decreased barrier thickness (Figs. 4.7 (e) and (f)) [publications IV and V].

Relaxation of carriers from a higher energy state to a lower state (carrier feeding) plays an important role in this kind of a multilevel energy structure. Basically, the levels are emptied one by one starting from the highest energy level. As reported for InGaAs/GaAs SIQDs, carrier feeding can cause somewhat similar plateau-like behavior [17] as seen in Fig. 4.7. However, it was pointed out in publication V that carrier feeding alone does not explain the evident dependency of the carrier lifetime on the barrier thickness observed in Fig. 4.7. Moreover, the fact that decreasing the barrier thickness results in a shorter decay time for both the QD0 and QW levels indicates that the increased non-radiative recombination in the QW and QDs is caused by surface-related effects. It seems likely that carriers might be captured by the stressor islands on the surface due to the lower band gap of InAs. Carriers in the islands could then recombine radiatively or experience non-radiative recombination via surface states. For simplicity, in the following, these processes are referred to as surface capture.

In the latter part of the QD0 curves, carrier feeding from the higher energy level becomes more and more insignificant meaning that the decay time is mostly determined by the radiative recombination and surface capture. Thus, the decay time constant determined from the experimental PL curve defines the lower limit for the time constant of the radiative recombination. For example, with a barrier thickness of 7 nm this lower limit is 0.8 ns.

As mentioned previously, the time-resolved PL of the InGaAs/GaAs SIQDs utilizing InP stressors has been shown to be unaffected by the variation of the barrier thickness. The QW PL intensity, however, was reported to diminish with decreased barrier thickness. Since the InP layer has been reported to passivate the GaAs surface [28], it has been presumed that the InP islands protect the strain-induced QD [19]. On the other hand, it has been reported that the surface depletion is suppressed and that surface band bending occurs in the region beneath the InAs/InP and the InAs/GaAs islands [57–59]. Same studies have shown, however, that an InAs wetting layer does not have such a significant effect. Since between the InAs stressor islands on InP there is most likely a thin InAs wetting layer, the effect of the wetting layer was also discussed in publication V. Near-surface QW structures (similar to the ones in SIQDs) were used as reference samples. Instead of growing InAs islands, only a thin layer of InAs was deposited on the surface to form a wetting layer without islands. A near-surface QW with no InAs was also fabricated for reference. TRPL transients of the samples with or the samples without the InAs wetting layer were virtually the same. This showed that wetting does not increase surface recombination significantly. With these observations, it was concluded in publication V

that the carriers captured away from the QW and QDs are mostly tunneled to the InAs islands on the surface.

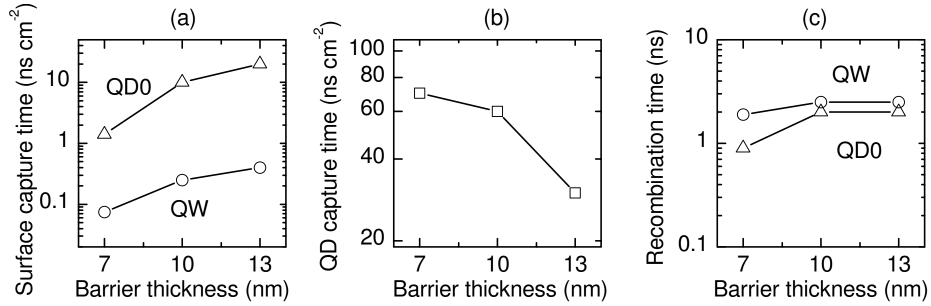

Figure 4.8. (a) Surface capture time constants, (b) QD capture time constants and (b) recombination time constants obtained for the QW and the QD0 from the rate equation model.

Figs. 4.8 (a) and (b) show surface capture and QD capture time constants obtained from the rate equation analyses in publications IV and V. Surface capture time constant increases (i.e., the capture probability decreases) by an order of magnitude as the barrier thickness is increased from 7 to 13 nm. It should be also noted that the probability of an electron to experience surface capture from the QW is over ten times larger as compared to the QD. As mentioned in chapter 4.1.2, 80 – 90 % of the redshift originates from the conduction band [publication III]. Thus, in the InGaAsP/InP QDs studied in publication V, the QW ground state for an electron is approximately 50 meV higher than the QD ground state (redshift is ∼55 meV). In other words, spatially under the stressor, an electron at the QW ground state experiences effectively ∼50 meV smaller barrier to the surface. This difference in the barrier height provides a plausible explanation for the smaller surface capture time constant observed for the QW compared to that of the QD0 in Fig. 4.8 (a).

The recombination time constants of the QD0 and QW peaks in Fig. 4.8 (c) do not show any significant dependence on the barrier thickness. The recombination time constant reported for InGaAs/GaAs SIQDs (0.86 ns [14]) is roughly the same as determined for InGaAsP/InP SIQDs with a barrier thickness of 7 nm in publication V (0.9 ns). Moreover, it also agrees with the lower limit (0.8 ns) determined above from the experimental TRPL measurement.

4.2 InAs nanorings on InP

4.2.1 Fabrication of self-assembled nanorings

It was previously reported in this thesis that the growth of InAs islands on InP was affected by the As/P exchange. It caused an undesired increase in the height of the islands. The As/P exchange process can, however, also be exploited in the fabrication of self-assembled structures. Instead of relying on the typical partial capping approach of nanoring fabrication, annealing in TBP was demonstrated to transform uncapped self-assembled InAs islands on InP into NRs in publication VI. This novel fabrication method is advantageous since the capping layer is no longer an integral part of the transformation process. Therefore, the transformation and capping can be optimized individually. Altogether, this potential can be capitalized in the investigation and design of NR structures and devices.

The fabrication process to create nanorings by annealing self-assembled islands introduced in this thesis is as follows. After the semi-insulating InP(001) substrate was annealed for 5 min at 650 °C, a 100-nm InP buffer layer was grown at 640 °C. Self-assembled islands were subsequently grown by depositing 0.6 – 1.0 MLs of InAs at 560 °C. Islands were then stabilized in TBAs for 10 s. In order to transform islands to rings the TBAs flow was switched to TBP. Reference samples were also fabricated by cooling down the deposited islands in TBAs (as-grown islands). [publication VI]

Fig. 4.9 (a) shows AFM images of the reference as-grown islands (top) and NRs formed utilizing a TBP anneal at 560 °C for 9 s (bottom). The difference in the morphology of an island (dotted line) and a NR (solid line) can be seen more clearly in the cross-sectional AFM profiles in Fig. 4.9 (b). The height of the island is approximately 30 nm whereas the height of the NR is only 10 nm. Moreover, it should be noted that the NR shows a distinct center hole with a diameter comparable to the island width (∼90 nm). This indicates that most of the island material has moved outward from the initial island location. Although the lateral sizes of the features are somewhat exaggerated due to the finite curvature of the AFM tip, the island and NR volumes were estimated to be roughly the same in publication VI. The areal density of the nanorings (and the islands) was typically $\sim 10^8$ cm^2.

The following conclusions were made in publication VI concerning the island-to-ring transformation process applied in this thesis compared to the previous studies (reviewed in section 3.3): Since no capping is applied, the

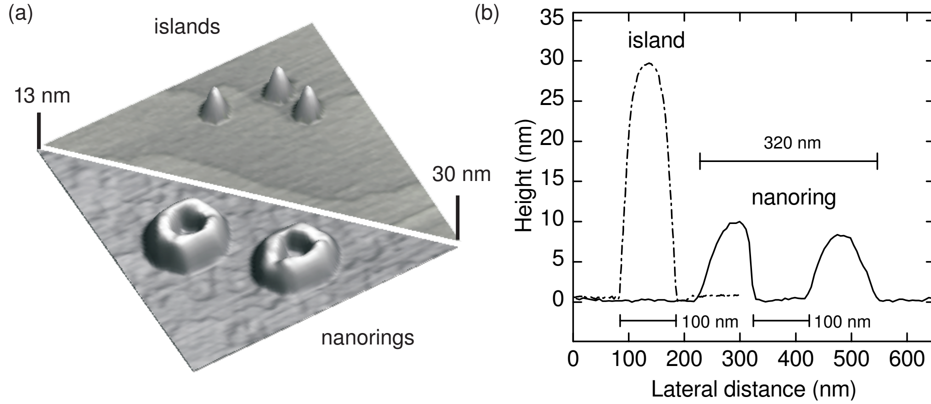

Figure 4.9. (a) Atomic force micrographs (1.4 µm × 1.4 µm) of InAs islands (top) and NRs (bottom). Note the different vertical scales. (b) AFM cross-section profiles of an InAs island (dotted line) and a NR (solid line).

thermodynamic model (which is based on the changes in surface free energy caused by the cap layer) was not considered to provide a plausible explanation for the transformation. The difference in group III surface mobilities (kinetic model [42, 43, 45]) does not provide an explanation either, because both materials have the same group III atom in the InAs/InP system.

Interestingly, the partial capping technique has also been used to fabricate InAs/InP NRs [44]. The kinetic model proposed for InAs/GaAs NRs was found to disagree with the results. Thus, the shape transformation was considered to be explained by the thermodynamic model. It should be mentioned that As/P exchange was not considered in that report in any way.

The As/P exchange has been shown to have a strong effect on InAs nanostructures on InP [49, 52, 60]. Furthermore, Ga atoms have been shown to migrate away from the top surface of partially relaxed InAs/GaAs islands due the chemical potential [48]. SiGe/Si [47] and InAs/InP [49] NR studies utilizing partial capping technique have also shown the significance of the strain distribution in the transformation process. Thus, it is conceivable that InP formed at the surface of InAs island by As/P exchange would experience strain-driven migration away from the island [publication VI].

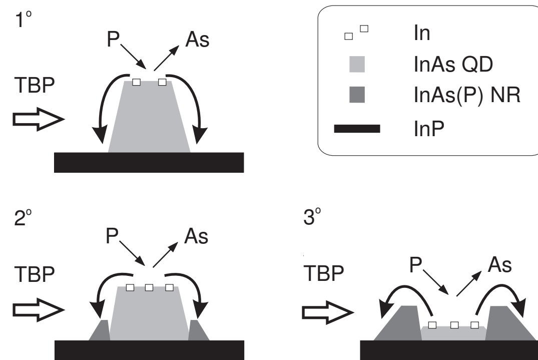

Figure 4.10. Schematic diagram of the island-to-ring transformation of an InAs/InP island by TBP annealing.

Based on these observations, a NR formation mechanism shown schematically in Fig. 4.10 was proposed in publication VI. (1°) Strain-driven migration concurrent with the As/P exchange moves In atoms outwards from the InAs island. (2°) In atoms are re-incorporated at an energetically more favorable (InP-like) site. (3°) Material redistribution continues until the initial InAs island has disappeared. The resulting NRs were assumed to consist of ternary $InAs_yP_{1-y}$, due to the As/P exchange processes.

Finally, it should be noted that in order to determine the exact mechanisms behind this transformation process further investigation including, e.g., detailed *in situ* monitoring and computational analysis would be required.

4.2.2 Island-to-ring evolution

In publication VII, the evolution of the island-to-ring transformation was studied by varying the maximum temperature and the duration of TBP annealing.

In addition to the fabrication process described above, temperature rampdown to 400 $^{\circ}$C was utilized before the TBP anneal at 520-555 $^{\circ}$C to assure that the (stabilized) islands would be as identical as possible in different growth runs right before the actual transformation process. Fig. 4.11 shows the morphological island-to-ring evolution achieved by varying the maximum temperature of the annealing step. A micrograph of an as-grown InAs

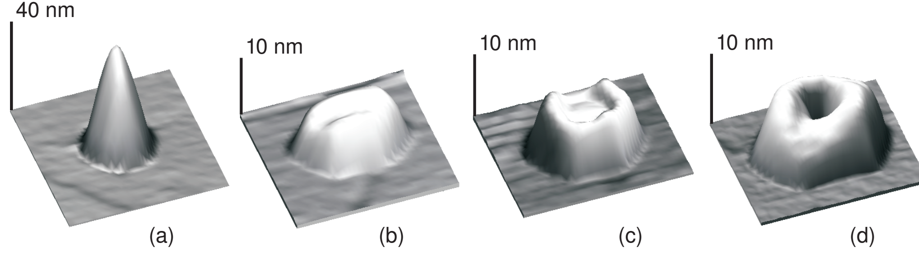

Figure 4.11. Atomic force micrographs (0.5×0.5 μm^2) of (a) as-grown InAs island, and island annealed in TBP at (b) 520, (c) 540, and (d) 555 °C. Note the different height scales.

island is shown in Fig. 4.11 (a). Fig. 4.11 (b) shows an island annealed at 520 °C. It can be observed that the height (∼10 nm) is clearly reduced while the diameter is increased notably. It seems that the island material is distributed around the original island location. Fig. 4.11 (c) shows that the formation of the center hole has started during the TBP anneal at 540 °C. A distinct NR seen in Fig. 4.11 (d) results from the annealing step at 555 °C. [publication VII]

The morphological evolution was studied in publication VII by varying the duration of the annealing step. Fig. 4.12 (a) shows the cross-sectional AFM profiles of the samples annealed at 550 °C for 12, 18, and 35 s. The height of the island is already reduced after 12 s of annealing, but the top surface is still quite flat. It resembles the island shown in Fig. 4.11 (b). However, a notable transformation towards NR profile is produced by 18 s of TBP annealing. Finally, the center hole extends to the surrounding buffer level after 35 s of annealing. This shows that most of the material from the initial InAs island has been redistributed.

Optical properties of the NRs were also studied in publication VII. A similar set of samples as characterized in Fig. 4.12 (a) was fabricated for the PL measurements by growing a 20-nm InP capping layer on top of the NRs. Fig. 4.12 (b) shows PL spectra of the samples with a varied annealing time (12, 18, and 35 s). It should be noted that the Ge detector used in the measurements cuts off most of the luminescence below 0.75 eV (the area is indicated with shading in Fig. 4.12 (b)). Nevertheless, it can be observed that the PL is blueshifted along with increased anneal time. It was concluded in publication VII that since the height of the NRs does not change significantly after 12 s of annealing, the blueshift occurs likely

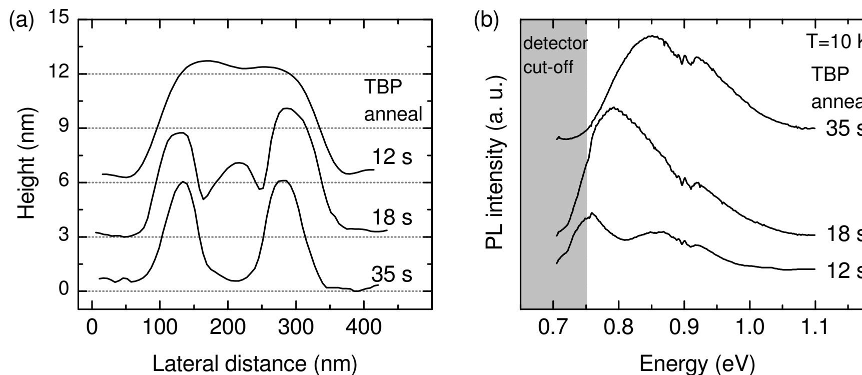

Figure 4.12. (a) AFM cross-section profiles and (b) PL spectra of NRs fabricated at 550 °C with a varied TBP anneal time. The shaded area on the left represents the response cut-off region of the Ge detector. The curves are offset vertically for clarity.

due to a compositional change in the NR material. It is conceivable that the low-energy side of the luminescence might originate from the As-rich region while the P-rich region is responsible for the high-energy luminescence. These observations support the assumption made in publication VI that the transformation of an InAs/InP island into a NR is accompanied by a compositional change of InAs to InAsP.

4.3 GaN passivation of GaAs surface

GaN is a wide band gap (3.4 eV) III-V semiconductor and it is considered to have a rather high thermal and chemical stability. It is very attractive material since it can be used to fabricate, e.g., blue LEDs and laser diodes [61, 62]. Typically, hexagonal GaN is grown on a sapphire substrate at temperatures around 1000 °C [63, 64]. On the other hand, cubic GaN can been grown on GaAs(100) substrates using temperatures around 550 °C [65, 66]. However, threading dislocations inflicted by the large lattice mismatch (∼20 %) between GaN and GaAs are problematic since they destroy the characteristics of the devices in most cases. This problem can be avoided by using ultrathin layers (few monolayers) of GaN, which are below the so-called critical thickness. This kind of ultrathin layer is not suitable for most of the optoelectronic applications. However, the stability of GaN can

be still exploited by using it, e.g., as a protective passivation layer on top of a structure to prevent surface recombination of charge carriers.

Different passivation techniques have been studied in order to reduce the density of surface states. GaP formed by As-P exchange reaction, native oxides, standard Si-based insulators (SiO_2 and Si_3N_4), and a variety of plasma nitridation methods have been demonstrated to passivate GaAs surfaces [67, 68]. The use of different plasma methods has faced problems with, e.g., disordered surface leading to deep donor states, and formation of mixture of GaN and Ga_2O_3 instead of pure GaN [69].

Passivation techniques using plasma are *ex situ* methods for most of the MOVPE systems. Although *ex situ* methods are useful if the structures are to be processed anyway, *in situ* surface passivation has been considered to be the most effective way to reduce the surface state density of epitaxial layers. For example, only 1 ML of InP has been shown to be effective in the passivation of AlGaAs/GaAs near-surface QWs [70–72]. Moreover, as mentioned previously, the InGaAs/GaAs SIQDs experience virtually no surface recombination due to the protective nature of the InP stressor islands [19].

MOVPE growth of epitaxial GaN on GaAs is enabled by the use of dimethylhydrazine as a nitrogen source. The low decomposition temperature of DMHy allows growth at temperatures around 550 °C [73]. Hence, the active structure will not suffer from additional heating during the passivation as the typical growth temperature of the GaAs-based materials is around 650 °C. In publication IX, the passivation of the GaAs surface by an epitaxial ultrathin GaN layer was studied. The growth procedures of GaN on GaAs [66], on the other hand, were based on the results of publication VIII.

A rather straightforward and sensitive method to assess the effect of the passivation is to optically probe the characteristics of a near-surface QW. Carriers from the near-surface QW are tunneled quite easily into possible surface states and that can be observed as a reduction of the PL intensity. As a result, while using identical near-surface QWs in a set of samples, the PL intensity gives an indication about efficiency of the passivation. In publication IX low-temperature photoluminescence was used to study the effect of passivation on InGaAs/GaAs near-surface QWs. Fig. 4.13 (a) shows the schematic structure of a passivation sample.

Prior to the growth of the QW structures, semi-insulating GaAs(100) substrates were annealed in the MOVPE reactor at 700 °C for 5 min to remove the native oxide. The $In_xGa_{1-x}As$ QW was fabricated at 650 °C on a 100-nm-thick GaAs buffer layer and was capped by 5 nm of GaAs. The thickness

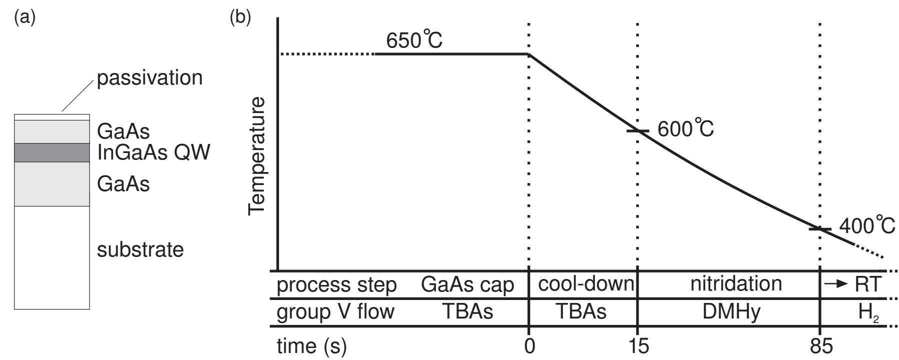

Figure 4.13. (a) Near-surface QW structure used in passivation samples and (b) schematic plot of the post-growth nitridation procedure (axes not in scale).

of the QW was 4 or 6 nm and the indium fraction x used was 20 or 25 %, respectively. Finally, the passivation layer was grown.

In publication VIII, a 5-period GaN/GaAs superlattice was used as a test structure in order to investigate the growth of GaN layers. A two-temperature growth process was found to yield good crystal quality and atomically flat surfaces. Based on these results, two different surface passivation methods using DMHy were employed.

In the first method, a thin GaN layer (nominally 1 – 3 MLs) was grown at 550 °C. In the second method, shown in Fig. 4.13 (b), after the growth of the top barrier GaAs layer, the TBAs flow was switched to DMHy at 600 °C to form a thin GaN layer via arsenic-to-nitrogen (As/N) exchange. After approximately 70 s of cooling, the DMHy protection was switched off at 400 °C. For reference, a similar near-surface QW structure was grown without passivation. A deep-QW sample with a 20-nm-thick GaAs top barrier layer was also used as a reference.

It was observed in publication IX that the PL intensity of the as-grown GaN passivated sample was enhanced by a factor of 21 compared to the unpassivated QW. Moreover, the integrated intensity of the as-grown GaN-passivated sample was nearly the same as compared to the deep QW sample. This indicates that the ultrathin GaN layer passivates the GaAs surface effectively.

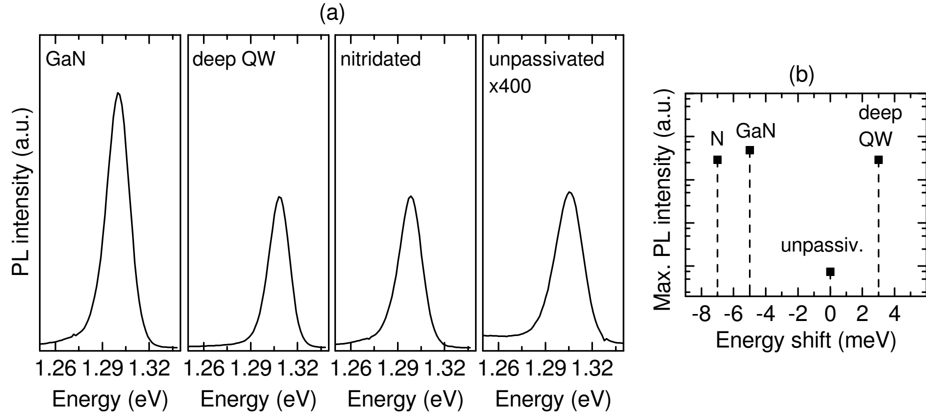

Figure 4.14. (a) PL spectra of passivated 4-nm-thick near-surface $In_{0.25}Ga_{0.75}As/GaAs$ QWs after storing samples about five months in ambient air. (b) Maximum PL intensities and the energy shift of the PL peaks extracted from the PL spectra in (a).

PL measurements for the same near-surface QWs were also carried out after storing the samples for about five months in ambient air. The PL spectra are shown in Fig. 4.14 (a). The PL intensity of the GaN-passivated sample is nearly 10^3 times larger compared to the unpassivated QW. The intensities of the nitridated and deep-QW structures are nearly the same. The photoluminescence of the deep InGaAs/GaAs QWs should not typically be affected by oxidation. Therefore, the results imply that nitridation and GaN passivation have protected the samples against degradation caused by oxidation. Overall, the PL intensity enhancement show that both the epitaxial GaN and the nitridation passivate the GaAs surface and this effect lasts over time.

In Fig. 4.14 (b) a redshift of $\sim$5 meV can be seen in the PL spectrum of the GaN passivated QW compared to the unpassivated structure. This behavior is probably caused by the formation of $GaAs_xN_{1-x}$ on the GaAs-GaN interface due to As/N exchange. As a consequence, the nominally 5-nm-thick top barrier GaAs has a graded composition of GaAsN. Thus, the QW barrier is presumably reduced because with low fractions of nitrogen, $GaAs_xN_{1-x}$ has a lower band gap than GaAs. This is seen as a redshift of the PL spectrum. These assumptions are supported by the fact that even a larger redshift ($\sim$7 meV) is evident in the spectrum of $In_xGa_{1-x}As/GaAs$ QW passivated with the nitridation method. While growing the GaN layer, the GaAs surface is exposed to nitrogen only a short period of time. In

the nitridation, on the other hand, the GaAs surface is exposed during the whole process allowing more effective As/N exchange on the surface. This means that in the nitridation process more nitrogen is diffused deeper into the GaAs barrier, effectively leading to even larger reduction of the QW barrier.

It was also noted in publication IX that the AFM micrographs showed no significant differences between the epitaxial GaN layer and the nitridated GaAs surface. Moreover, the passivation treatments do not seem to degrade the surface morphology of the GaAs. All in all, the results in publication IX suggest that the ultrathin epitaxial GaN layer grown on GaAs is an efficient *in situ* method for surface passivation.

5 Summary

Self-assembled nanostructures are of particular interest in semiconductor technology, since they have novel quantum mechanical properties and they offer new functionality or improved performance for applications. A typical approach is to bury self-assembled islands in another semiconductor with a larger band gap to create QDs, which are applicable, e.g., in optoelectronics. Alternatively, self-assembled islands can be used as stressors on top of a near-surface QW in order to create strain-induced QDs or stressor QDs within the QW.

In this thesis, the main focus was in the fabrication and characterization of self-assembled III-V compound semiconductor nanostructures. Firstly, self-assembled InAs islands were used to produce stressor QDs. Secondly, InAs islands were transformed into nanorings. Thirdly, *in situ* grown epitaxial GaN layers were used to passivate GaAs surfaces. The samples studied in this thesis were fabricated by MOVPE. AFM was used to study the size and areal density of the InAs islands as well as the morphology of the nanorings. Low-temperature PL measurements were used to study the optical characteristics of the samples.

A new material system utilizing InAs stressor islands to create InGaAs(P)/InP strain-induced QDs was demonstrated. The wavelength of the QD ground state luminescence was tuned in the range of 1.3 – 1.7 µm by varying the QW composition. The island ensemble was optimized using a temperature ramp-down to reduce the uncontrolled accumulation of material trough arsenic-to-phosphorus exchange. Modification of the QD confinement potential by varying the height of the islands (from 15 to 30 nm) or by decreasing the distance of the QW from the surface (from 13 to 4 nm) was observed to increase the energy separation (PL redshift) of the QD and QW ground states approximately by 20 meV. Moreover, it was found that the most feasible size of the stressor islands is around 15 to 30 nm in height. Based on the time-resolved PL measurements, it was concluded that the lifetime of carriers in the QD was reduced by the carrier capture of

stressor islands on the surface. However, the results show that the surface capture rate can be decreased considerably by controlling the distance of the QW from the surface. All in all, PL spectra showed a typical spacing of 15 meV between the QD peaks, a FWHM as narrow as 11 meV for the QD peaks, and a redshift of the QD ground state peak from the QW peak as large as 70 meV.

Previously, self-assembled nanorings have been typically fabricated by transforming self-assembled islands into nanorings utilizing a partial capping layer and a subsequent annealing step. In the method introduced in this thesis, however, no capping was used. Instead, the island-to-ring transformation was achieved by annealing the self-assembled InAs islands in a phosphorous ambient. It was assumed that the material redistribution, i.e., the transformation, was caused by the arsenic-to-phosphorus exchange along with the strain-driven migration of In atoms outwards from the island.

Passivation of a GaAs surface by an epitaxial ultrathin GaN layer was studied in order to reduce the density of surface states. The GaN layers were grown *in situ* on the top of near-surface InGaAs/GaAs QWs. The effect of the surface passivation was determined by comparing the PL intensities. Significant enhancement of the PL intensity due to passivation showed that the ultrathin epitaxial GaN layer grown on GaAs is an efficient method for surface passivation.

References

[1] M. E. Heimbuch, A. L. Holmes, Jr., C. M. Reaves, M. P. Mack, S. P. DenBaars, and L. A. Coldren, J. Electron Mater. **23**, 87 (1994).

[2] G. Binning, C. F. Quate, and C. Gerbe, Phys. Rev. Lett. **56**, 930 (1986).

[3] G. W. Bryant, Phys. Rev. B **37**, 8763 (1988).

[4] F. C. Frank and J. H. van der Merwe, Proc. Roy. Soc. London **A198**, 216 (1949).

[5] M. Volmer and A. Weber, Z. Physik. Chem. **119**, 277 (1926).

[6] I. N. Stranski and L. Krastanow, Sitz. Ber. Akad. Wiss., Math.-naturwiss. Kl. Abt. IIb **146**, 797 (1938).

[7] D. J. Eaglesham and M. Cerullo, Phys. Rev. Lett. **64**, 1943 (1990).

[8] M. A. Reed, R. T. Bate, K. Bradshaw, W. M. Duncan, W. R. Frensley, J. W. Lee, and H. D. Shih, J. Vac. Sci. Technol. B **4**, 358 (1986).

[9] K. Kash, A. Scherer, J. M. Worlock, H. G. Craighead, and M. C. Tamargo, Appl. Phys. Lett. **49**, 1043 (1986).

[10] K. Kash, J. M. Worlock, M. D. Sturge, P. Grabbe, J. P. Harbison, A. Scherer, and P. Lin, Appl. Phys. Lett. **53** (1988).

[11] M. Sopanen, H. Lipsanen, and J. Ahopelto, Appl. Phys. Lett. **66**, 2364 (1995).

[12] H. Lipsanen, M. Sopanen, and J. Tulkki, a review chapter 4 *Optical Properties of Quantum Dots Induced by Self-Assembled Stressors* in *Optics of Quantum Dots and Wires*, edited by G. W. Bryant and G. S. Solomon (Artech House Inc., Norwood, MA, USA, 2005).

[13] J. Tulkki and A. Heinämäki, Phys. Rev. B **51**, 8239 (1995).

[14] M. Brasken, M. Lindberg, and J. Tulkki, phys. stat. sol. A **164**, 427 (1997).

[15] U. Bockelmann and T. Egeler, Phys. Rev. B **46**, 15574 (1992).

[16] M. Brasken, M. Lindberg, M. Sopanen, H. Lipsanen, and J. Tulkki, Phys. Rev. B **58**, R15993 (1998).

[17] S. Grosse, J. H. H. Sandmann, G. von Plessen, J. Feldmann, H. Lipsanen, M. Sopanen, J. Tulkki, and J. Ahopelto, Phys. Rev. B **55**, 4473 (1997).

[18] H. Lipsanen, M. Sopanen, and J. Ahopelto, Phys. Rev. B **51**, 13868 (1995).

[19] C. Lingk, W. Helfer, G. von Plessen, J. Feldmann, K. Stock, M. W. Feise, D. S. Citrin, H. Lipsanen, M. Sopanen, R. Virkkala, J. Tulkki, and J. Ahopelto, Phys. Rev. B **62**, 13588 (2000).

[20] M. Grundmann, R. Heitz, D. Bimberg, and J. H. H. Sandmann, phys. stat. sol. (b) **203**, 121 (1997).

[21] J. Ahopelto, M. Sopanen, and H. Lipsanen, Jpn. J. Appl. Phys. **38**, 1081 (1999).

[22] H. Koskenvaara, T. Hakkarainen, H. Lipsanen, and M. Sopanen, J. Mat. Sci. **14**, 357 (2003).

[23] M. Sopanen, M. Taskinen, H. Lipsanen, and J. Ahopelto, Appl. Phys. Lett. **69**, 3393 (1996).

[24] M. C. Hanna, Z. H. Lu, A. F. Cahill, M. J. Heben, and A. J. Nozik, J. Cryst. Growth **174**, 605 (1997).

[25] T. Wang and A. Forchel, Appl. Phys. Lett. **73**, 1847 (1998).

[26] E. S. Kim, N. Usami, and Y. Shiraki, Appl. Phys. Lett. **70**, 295 (1997).

[27] W. V. Schoenfeld, C. Metzner, E. Letts, and P. M. Petroff, Phys. Rev. B **63**, 205319 (2001).

[28] H. Lipsanen, M. Sopanen, M. Taskinen, J. Tulkki, and J. Ahopelto, Appl. Phys. Lett. **68**, 2216 (1996).

[29] T. Wang and A. Forchel, J. Appl. Phys. **86**, 2001 (1999).

[30] N. N. Ledentsov, J. Böhrer, M. Beer, F. Heinrichsdorff, M. Grundmann, D. Bimberg, S. V. Ivanov, B. Y. Meltser, S. V. Shaposhnikov, I. N. Yassievich, N. N. Faleev, P. S. Kop'ev, and Zh. I. Alferov, Phys. Rev. B **52**, 14058 (1995).

[31] M. Bayer, M. Korkusinski, P. Hawrylak, T. Gutbrod, M. Michel, and A. Forchel, Phys. Rev. Lett. **90**, 186801 (2003).

[32] Y. Aharonov and D. Bohm, Phys. Rev. **115**, 485 (1959).

[33] D. Mailly, C. Chapelier, and A. Benoit, Phys. Rev. Lett. **70**, 2020 (1993).

[34] R. J. Warburton, C. Schäflein, D. Haft, A. L. F. Bickel and, K. Karrai, J. M. Garcia, W. Schoenfeld, and P. M. Petroff, Nature **405**, 926 (2000).

[35] A. Lorke, R. J. Luyken, A. O. Govorov, J. P. Kotthaus, J. M. Garcia, and P. M. Petroff, Phys. Rev. Lett. **84**, 2223 (2000).

[36] F. Suárez, D. Granados, M. L. Dotor, and J. M. García, Nanotechnology **15**, S126 (2004).

[37] A. Y. Nazzal, H. Fu, and L.-W. Wang, J. Appl. Phys. **98**, 083703 (2005).

[38] P. A. Orellana and M. Pacheco, Phys. Rev. B **71**, 235330 (2005).

[39] T. Chakraborty and P. Pietiläinen, Phys. Rev. B **50**, 8460 (1994).

[40] T. W. Kim, E. H. Lee, K. H. Lee, J. S. Kim, and H. L. Park, Appl. Phys. Lett. **84**, 595 (2004).

[41] S. Kobayashi, C. Jiang, T. Kawazu, and H. Sakaki, Jpn. J. Appl. Phys. **43**, L662 (2004).

[42] A. Lorke, R. Blossey, J. M. Garcia, M. Bichler, and G. Abstreiter, Mat. Sci. Eng. B **88**, 225 (2002).

[43] A. Lorke, R. J. Luyken, J. M. Garcia, and P. M. Petroff, Jpn. J. Appl. Phys. **40**, 1857 (2001).

[44] T. Raz, D. Ritter, and G. Bahir, Appl. Phys. Lett. **82**, 1706 (2003).

[45] J. M. Garcia, G. Medeiros-Ribeiro, K. Schmidt, T. Ngo, J. L. Feng, A. Lorke, J. Kotthaus, and P. M. Petroff, Appl. Phys. Lett. **71**, 2014 (1997).

[46] R. Blossey and A. Lorke, Phys. Rev. E **65**, 021603 (2002).

[47] J. Cui, Q. He, X. M. Jiang, Y. L. Fan, X. J. Yang, F. Xue, and Z. M. Jiang, Appl. Phys. Lett. **83**, 2907 (2003).

[48] Q. Xie, P. Chen, and A. Madhukar, Appl. Phys. Lett. **65**, 2051 (1994).

[49] P. J. Poole, R. L. Williams, J. Lefebvre, and S. Moisa, J. Cryst. Growth **257**, 89 (2003).

[50] S. Yoon, Y. Moon, T.-W. Lee, E. Yoon, and Y. D. Kim, Appl. Phys. Lett. **74**, 2029 (1999).

[51] B. Wang, F. Zhao, Y. Peng, Z. Jin, Y. Li, and S. Liu, Appl. Phys. Lett. **72**, 2433 (1998).

[52] H. R. Gutiérrez, M. A. Cotta, J. R. R. Bortoleto, and M. M. G. de Carvalho, J. Appl. Phys. **92**, 7523 (2002).

[53] W. Seifert, N. Carlsson, J. Johansson, M.-E. Pistol, and L. Samuelson, J. Cryst. Growth **170**, 39 (1997).

[54] N. Carlsson, T. Junno, L. Montelius, M.-E. Pistol, L. Samuelson, and W. Seifert, J. Cryst. Growth **191**, 347 (1998).

[55] M. A. Cotta, C. A. C. Mendonca, E. A. Meneses, and M. M. G. Carvalho, Surf. Sci. **388**, 84 (1997).

[56] P. Jin, X. Q. Meng, C. M. L. Z. Y. Zhang, F. Q. L. B. Xu, Z. G. Wang, Y. G. Li, C. Z. Zhang, and S. H. Pan, J. Appl. Phys. **93**, 4169 (2003).

[57] K. O. Vicaro, M. A. Cotta, H. R. Gutiérrez, and J. R. R. Bortoleto, Nanotech. **14**, 509 (2003).

[58] I. Tanaka, I. Kamiya, H. Sakaki, N. Qureshi, J. S. J. Allen, and P. M. Petroff, Appl. Phys. Lett. **74**, 844 (1999).

[59] T. Takahashi, M. Yoshita, I. Kamiya, and H. Sakaki, Appl. Phys. A **66**, S1055 (1998).

[60] M. Taskinen, M. Sopanen, H. Lipsanen, J. Tulkki, T. Tuomi, and J. Ahopelto, Surf. Sci. **376**, 60 (1997).

[61] S. Nakamura, J. Mater. Res. **14**, 2716 (1999).

[62] T. Mukai and S. Nakamura, Jpn. J. Appl. Phys **38**, 5735 (1999).

[63] I. Akasaki, H. Amano, Y. Koide, K. Hiramatsu, and N. Sawaki, J. Crystal Growth **98**, 209 (1989).

[64] K. Hiramatsu, S. Itoh, H. Amano, I. A. Kuwano, T. Shiraishi, and K. Oki, J. Cryst. Growth **115**, 628 (1991).

[65] H. Yang, O. Brandt, A. Trampert, and K. H. Ploog, Appl. Surf. Sci. **104/105**, 461 (1996).

[66] J. Sormunen, J. Toivonen, M. Sopanen, and H. Lipsanen, Appl. Surf. Sci. **222**, 286 (2004).

[67] M. Losurdo, P. Capezzuto, and G. Bruno, Appl. Phys. Lett. **81**, 16 (2002).

[68] S. Anantathanasarn and H. Hasegawa, Appl. Surf. Sci. **190**, 343 (2002).

[69] S. Anantathanasarn, S.-Y. Oomoto, T. Hashizume, and H. Hasegawa, Appl. Surf. Sci. **159/160**, 456 (2000).

[70] Y. Wada and K. Wada, Appl. Phys. Lett. **63**, 379 (1993).

[71] Y. Wada and K. Wada, J. Vac. Sci. Technol. B **12**, 3084 (1994).

[72] H. Lipsanen, M. Sopanen, M. Taskinen, J. Tulkki, and J. Ahopelto, Appl. Phys. Lett. **68**, 2216 (1996).

[73] H. Sato, H. Takahashi, A. Watanabe, and H. Ota, Appl. Phys. Lett. **68**, 3617 (1996).